Convection, Thermal Bifurcation, and the Colors of A Stars

Theodore Simon[1]
Institute for Astronomy, University of Hawaii, 2680 Woodlawn Drive, Honolulu, HI 96822

and

Wayne B. Landsman[1]
Hughes STX Corp., NASA/GSFC, Code 681, Greenbelt, MD 20771

ABSTRACT

Broad-band ultraviolet photometry from the *TD-1* satellite and low dispersion spectra from the short wavelength camera of *IUE* have been used to investigate a long-standing proposal of Böhm-Vitense that the normal main sequence A– and early–F stars may divide into two different temperature sequences: (1) a high temperature branch (and plateau) comprised of slowly rotating convective stars, and (2) a low temperature branch populated by rapidly rotating radiative stars. We find no evidence from either dataset to support such a claim, or to confirm the existence of an "A–star gap" in the $B-V$ color range $0.22 \leq B-V \leq 0.28$ due to the sudden onset of convection.

We do observe, nonetheless, a large scatter in the 1800–2000 Å colors of the A–F stars, which amounts to ~ 0.65 mags at a given $B-V$ color index. The scatter is not caused by interstellar or circumstellar reddening. A convincing case can also be made against binarity and intrinsic variability due to pulsations of δ Sct origin. We find no correlation with established chromospheric and coronal proxies of convection, and thus no demonstrable link to the possible onset of convection among the A–F stars. The scatter is not instrumental. Approximately 0.4 mags of the scatter is shown to arise from individual differences in surface gravity as well as a moderate spread (factor of ~ 3) in heavy metal abundance and UV line blanketing. A dispersion of ~ 0.25 mags remains, which has no clear and obvious explanation. The most likely cause, we believe, is a residual imprecision in our correction for the spread in metal abundances. However, the existing data do not rule out possible contributions from intrinsic stellar variability or from differential UV line blanketing effects owing to a dispersion in microturbulent velocity.

---

[1]Guest Observer with the *International Ultraviolet Explorer (IUE)* satellite

1. Introduction

Along the lower half of the main sequence, it is among the A-type stars that a shallow convection zone first appears in the outer envelope of low mass stars (e.g., Gilliland 1986). For a variety of observational and astrophysical reasons, it has proved quite difficult to find the precise location where, in terms of effective temperature, $B-V$ color, or spectral class, this structural change actually occurs. The primary spectral proxies for convection, namely, X-ray and near ultraviolet (UV) emission from hot coronal and chromospheric gas, suggest that convection is common, though perhaps not universal, among the late A–type and early F–type stars (hereinafter, A–F stars), but is much more infrequent among the middle–A stars (Simon & Landsman 1991; Simon, Drake, & Kim 1995). Why it is that some A or F stars are X-ray or UV emitters, and are thus demonstrably convective, while others are not, remains a mystery.

This perplexing issue was addressed in a series of articles begun nearly three decades ago by Böhm-Vitense (1982, hereinafter BV82, and references cited therein). A principal conclusion of those studies is that when main sequence convection first sets in among the A–F stars, it does so very abruptly. As a result of this change, according to Böhm-Vitense, there may be major effects on the spectral line profiles of a star (Böhm-Vitense 1970a), as well as pronounced changes in the overall spectral energy distribution. At visible wavelengths, within the Paschen continuum below 5000Å, for instance, the onset of convection makes a star look redder, and thus cooler, than it would otherwise appear in the absence of convection (Böhm-Vitense 1970b, 1978). And because the transformation is expected to take place over just a narrow range in mass, there is a large increase in the $B-V$ color for only a slight drop in the effective temperature, $T_{\rm eff}$. Consequently, in a plot of the observational main sequence as a function of $B-V$, a plateau in $T_{\rm eff}$ should appear in the midst of the A–F star range, extending from $B-V = 0.22$ to $B-V = 0.28$ (Böhm-Vitense & Canterna 1974; Böhm-Vitense 1981a, BV82).

The way in which these effects of convection alter A–F star spectra is either by modifying the temperature gradient in deep layers of the atmosphere (Böhm-Vitense 1978), or else through the mediation of photospheric granulation (BV82). Support for the latter explanation, cited in BV82, comes from numerical simulations by Nelson (1980), which suggest that the temperature and pressure inhomogeneities associated with a solar-type granulation pattern can redden the $B-V$ color of an A or early F star by as much as 0.07 mag. Modern studies of convection based on the analysis and modelling of spectral line bisectors all seem to imply, however, that the granulation patterns of these early stars and the Sun may bear very little resemblance to one another (e.g., Gray 1989, Dravins 1990).

Other work by Böhm-Vitense & Canterna (1974) and BV82 goes on to suggest that if

the incipient convection is weak, it may be suppressed by rapid rotation. Hence, rapidly rotating A–F stars should tend to stay radiative, exhibiting normal spectra and colors, while slowly rotating stars, offering no obstacle to convection, should tend to become convective and be shifted to redder $B-V$ colors. This differentiation based on rotation should therefore give rise to two distinct sequences of A–F stars in the H–R plane: (1) a high–$T_{\rm eff}$ branch populated by the slowly rotating, weakly convective stars, and, at the same $B-V$ colors, (2) a low–$T_{\rm eff}$ branch comprised of the rapidly rotating, purely radiative stars. Farther down the main sequence, once convection is much more firmly established among the middle and late F stars at $B-V \geq 0.30$, these two branches merge back together again to form a single temperature sequence.

The existence of a thermal bifurcation among the A–F stars provides, according to Böhm-Vitense (1970b) and Böhm-Vitense & Canterna (1974), a natural explanation for the deficiency some authors find in the numbers of late A stars relative to those of earlier and later spectral classes, both in the counts of stars in the solar neighborhood and also in cluster stars of various ages (e.g., Houk & Fesen 1978, Harris et al. 1993). In their view, it is the sudden onset of convection near $B-V = 0.22$, and the resulting shift in $B-V$ color, that creates this apparent "A–star gap". However, other observers (e.g., Kjeldsen & Frandsen 1991) report they are unable to confirm that such a gap truly exists.

A test of these ideas concerning the onset of convection and its observable effects on stellar energy distributions was presented in BV82. The analysis carried out there was based on the premise that (1) the main spectroscopic changes induced by convection are limited to visible wavelengths, and that (2) none of the effects of convective granulation predicted by Nelson's (1980) calculation can penetrate into the layers of the photosphere from which the UV spectrum of an A–F star emerges. Thus, the UV energy distribution of an A–F star, unlike its optical spectrum, should reflect the true $T_{\rm eff}$ of the star. In particular, from a consideration of theoretical model atmosphere fluxes, it was shown that the ratio of the apparent brightness of a star at 1900Å to its brightness at optical wavelengths (or the color index formed therefrom) provides a sensitive estimate of $T_{\rm eff}$, which is free of the effects that might arise with the onset of convection.

Narrow-band ($\sim$ 40Å resolution) fluxes measured at 1900Å by the S2/68 Sky Survey Telescope aboard the *TD–1* satellite (Jamar et al. 1976, Macau-Hercot et al. 1978) were used in BV82 to derive effective temperatures for a sample of A and F stars by comparison with a grid of model atmospheres. The resulting $T_{\rm eff}$ estimates were then plotted against the observed $B-V$ colors. In the diagram thus derived (see Figure 7 of BV82), Böhm-Vitense identified two branches of stars as we have just described them: an upper one comprised of slowly rotating, convective stars that have been shifted horizontally to the right in $B-V$

color to form a temperature "plateau," and a lower one occupied by rapidly rotating stars that have remained fully radiative. Our version of this diagram, which omits the high luminosity giants and bright giants included in the original plot, is shown here as Figure 1 (see also Saxner & Hammarbäck 1985).

Even at its widest separation, the vertical distance between the two temperature sequences is no greater than $\Delta T_{\rm eff} = 500$ K, which corresponds to a spread in UV flux of less than a factor of two. By comparison, the photometric errors in the narrow-band *TD–1* fluxes used in BV82 to construct this diagram range from 5% to more than 40%; fully one-third of the errors, as cataloged by Jamar et al. (1976) and Macau-Hercot et al. (1978), are above ±25%. Errors this large imply an uncertainty of at least ±180 K in the $T_{\rm eff}$ estimates of individual stars. Given uncertainties of this size, the reality of the proposed temperature plateau and temperature bifurcation was not, in our opinion, convincingly proved.

There are two additional reasons for caution that deserve mention here. First, for the same stars analyzed in BV82 by the UV method, independent estimates of $T_{\rm eff}$ can be derived from *uvbyβ* photometry (Moon & Dworetsky 1985; Napiwotzki, Schönberner, & Wenske 1993; Smalley & Dworetsky 1995). In a number of cases, this leads to a substantial disagreement in the $T_{\rm eff}$ estimates. As illustrated in Figure 1, some stars on the upper convective branch in BV82 belong on the lower radiative branch according to their *uvbyβ* photometry, while others should move in the opposite direction. These inconsistencies are substantial enough, we think, to raise doubt about whether the temperature gap suggested by the narrow-band *TD–1* photometry is entirely credible. Whether this apparent contradiction is actually significant depends, however, on the accuracy of the individual temperature estimates. Based on their ability to recover the $T_{\rm eff}$ of the fundamental stars used to calibrate their technique, Moon & Dworetsky (1985) estimate the external accuracy of their method to be no better than ±250 K, while similar evaluations have been cited by Smalley & Dworetsky (1993) and Napiwotzki et al. (1993). Such a large uncertainty significantly reduces the confidence with which a temperature differential amounting to $\Delta T_{\rm eff} = 500$ K might be detected by means of the *uvbyβ* photometry.

In addition, we note that while the effects of convection on stellar energy distributions and the resulting spread in photometric colors are presumed to be limited to the A–F stars, the issue of whether hotter or cooler stars show as great a spread in their photometry has not been systematically considered before. Figure 2 is a plot of the narrow-band 1900Å colors for the main sequence stars listed in Tables 1 and 2 of BV82. Also plotted are the colors predicted by ATLAS9 model atmospheres from Kurucz (1993a) for solar metallicity and $\log g = 4$, and offset parallel lines which demarcate a band ±0.4 mags wide above

and below on either side of the model sequence. As mentioned earlier, and as explained more fully in BV82, any vertical spread in the UV color index is equivalent to a spread in $T_{\rm eff}$. A considerable scatter is evident along the main sequence in the UV emission of stars on either side of the "A-star gap," both above it and below it. This is perhaps not surprising for the cooler stars at $B-V> 0.3$, given the increasing faintness of these stars in the UV and the greater complexity of their spectra due to line blanketing. On the other hand, it is harder to reconcile the dispersion shown by the hotter stars, considering that the scatter extends all the way up the main sequence to the earliest points plotted near $B-V= 0.0$, among stars for which there is no suspicion that convection is present. Scatter of similar amplitude, equivalent to 500 K in $T_{\rm eff}$, had already been noted before at $B-V< 0.1$ in narrow-band *TD–1* photometry at 1400Å and 2100Å by Malaise et al. (1974), who attributed it to individual variations in spectral line blanketing, and also in Am-type stars by van 't Veer-Menneret et al. (1980). Clearly, then, a number of causes other than convection (including observational errors) may need to be considered as possible explanations for the observed spread in the *TD–1* fluxes of the A- and F-type stars.

Given the apparent conflicts in stellar temperature estimates made independently from UV and optical photometry, and the scatter in UV flux present even among the fully radiative stars of Figure 2, we re-examine in this paper the related issues of the onset of convection and the effective temperature scale of the A–F stars — two important questions that were raised by Böhm-Vitense's pioneering studies. Initially we discuss our analysis of an enlarged sample of *TD–1* flux measurements for these stars, in which we make use of broad-band ($\sim$ 330Å) fluxes from *TD–1*. These data are generally much more accurate than the narrow-band fluxes used in BV82. We then go on to discuss narrow-band (20–40Å) spectrophotometry from the *IUE* telescope, which we obtained for a sample of A–F stars in the 1800–2000Å region. In this work we take advantage of the high sensitivity and photometric accuracy of *IUE*. All of the A or F stars that were observed only with great difficulty by *TD–1* are within the grasp of *IUE* in exposure times of just a few minutes, or even a few seconds. Moreover, the photometric uncertainties of the *IUE* data, both internal and external, are at a level of a few percent, corresponding to an accuracy of $\pm$25 K in $T_{\rm eff}$. This provides a vast improvement over the narrow-band *TD–1* spectrophotometry upon which Böhm-Vitense relied.

2. Spectrophotometry from *TD–1*

Using an electronic version of the Thompson et al. (1978) catalog, we extracted broad-band ($\Delta\lambda \approx$ 330Å) *TD–1* fluxes centered at 1965Å for more than 600 stars in

the *Yale Bright Star Catalogue* (Hoffleit & Jaschek 1982) with $B-V$ colors in the range $0.00 \leq B-V \leq 0.45$. From this initial list we eliminated all known Ap and Am stars, and any normal star with a cataloged flux error $> 10\%$. For each of the remaining 300+ stars we obtained Strömgren ($uvby\beta$) photometry either from the Hauck & Mermilliod (1990) catalog or from the SIMBAD database. We used this photometry to estimate $T_{\rm eff}$ in accordance with the method developed by Moon & Dworetsky (1985), which, for stars cooler than 8500 K, relies mainly on the Hβ index, β, to gauge the value of $T_{\rm eff}$. A plot of the temperatures determined in this way, restricted to those stars in our *TD–1* sample with colors in the range $0.15 \leq B-V \leq 0.33$, is shown in Figure 3. No obvious clustering of the stars into two separate temperature sequences is apparent here. However, considering the acknowledged uncertainty of ± 250 K in our temperature estimates, a gap of the size claimed by BV82 might well be hidden within the cloud of points plotted in Figure 3.

A more fundamental issue is whether one should expect to see evidence of a temperature bifurcation in a plot such as Figure 3, where both axes are potentially affected by convection. The profile of Hβ is known to be sensitive to the influence of convection (see, e.g., van 't Veer-Menneret & Mégessier 1996). According to Böhm-Vitense (1970a), "...stratification makes a convective star appear redder and the hydrogen lines somewhat weaker than in a radiative star of the same $T_{\rm eff}$. This still holds when temperature inhomogeneities in the convective star are considered. However, when comparing radiative and convective stars of the same $B-V$, they have almost the same hydrogen line strengths, but the convective star has a higher $T_{\rm eff}$." Simply put, Hβ and the $B-V$ color index are both subject to changes brought on by atmospheric convection. One therefore has to turn elsewhere, to the UV spectrum according to BV82, to see this physical transformation.

In our analysis of the broad-band *TD–1* fluxes, we follow basically the same approach taken in BV82, i.e., for each individual star we use the ratio of the broad-band 1965Å flux to the visible flux in order to impute a $T_{\rm eff}$. The difference is that we stay entirely within the observational plane instead of transforming the flux ratio (or equivalently the ultraviolet minus visible color index) into an explicit value of $T_{\rm eff}$. We write, [1965Å] $\equiv m(1965\text{Å}) - V$, where the UV magnitude is given as usual by $m(\lambda) = -2.5 \log f_\lambda - 21.10$, and $f_\lambda = f_{1965}$ is the tabulated *TD–1* flux. No adjustments have been made to the zero point of the *TD–1* flux scale, since Bohlin & Holm (1984) found excellent agreement between the *TD–1* and the IUESIPS flux scales near 1900 Å. The [1965Å] color index computed from the broad-band 1965Å flux of each star is plotted against $B-V$ color in Figure 4. For reference, we provide a temperature scale along the right-hand side of the graph, which shows the conversion from UV color to $T_{\rm eff}$, based on the fluxes predicted by ATLAS9 model atmospheres. In this color–color plot, the visibility of different sequences of convective or radiative stars is limited only by the formal errors in the ultraviolet photometry, which are 0.1 mag or

smaller. The corresponding uncertainty in the implied $T_{\rm eff}$ is ± 80 K or less, which should be sufficient to resolve a substantial temperature gap.[2]

The range in $B-V$ colors plotted in Figure 4 includes the "A–star gap." As in the previous figure, we see no indication in this plot for two distinct photometric sequences of stars, and no evidence for a drop in the numbers of stars in the color range $0.22 \leq B-V \leq 0.28$. A histogram of the cumulative star count, presented in Figure 5, shows a smooth and steady progression as a function of $B-V$ color, with no leveling off to indicate a decline in the number density of stars in the above color range. This result is only suggestive because the survey sample is roughly flux limited, rather than volume limited. Nevertheless, any selection effects in a flux-limited survey should be monotonic with $B-V$, and thus unlikely to affect the detectability of a gap in the stellar number density.

For a more quantitative statistical assessment, we have examined the distribution of [1965Å] as a function of $B-V$ color on either side of, and through, the domain of the "A–star gap." If the stars in any $B-V$ interval congregate into two separate temperature sequences, the distribution in their [1965Å] colors should appear bimodal. However, in no $B-V$ color interval do we find this to be the case, nor do we find any evidence that the variation in the mean or median UV color as a function of $B-V$ changes slope to reflect the possible presence of a "plateau" among the A or F stars. The mean value of [1965Å], computed for 0.01 mag intervals in $B-V$, is illustrated in Figure 6. According to a Kolmogorov-Smirnov (K–S) test, the trend in the average value of [1965Å], from $B-V=$ 0.15 to $B-V=$ 0.33, is indistinguishable from a straight line. The standard error in a linear least-squares fit is ± 0.07 mag; this corresponds to a full 1σ range in $T_{\rm eff}$ of 120 K, which is a factor of four smaller than the vertical distance separating the two branches of stars found in BV82.

Figure 6 also summarizes in box-plot format the change in the distribution of UV colors along the main sequence, for two $B-V$ color bins blueward, one bin within, and two bins redward of the "A–star gap." No plateau is apparent in the median value of [1965Å], or at any of the four other percentile levels depicted there. Our study of an extensive sample of broad-band *TD–1* photometry thus fails to confirm the existence of the temperature bifurcation and temperature plateau previously suggested by BV82 from her analysis of the

[2] The stars farthest from the model atmosphere curve in Figure 4 are HR 1104, HR 3113, and HR 3756. HR 3113 is a bright giant (Lemke 1989), whose location far below the main sequence relation is the result of its high luminosity, as we show later on. HR 1104 and HR 3756 are relatively bright at UV wavelengths, but *IUE* photometry fails to confirm their *TD–1* photometry, suggesting that these stars are either highly time variable or else their *TD–1* photometry is in error, perhaps due to source confusion in the $11' \times 18'$ entrance slot.

narrow-band photometry.

In a horizontally stratified atmosphere, the UV flux may emerge from a large range of heights, depending on the wavelength– and temperature–sensitivity of the opacity (Nordlund & Dravins 1990). Consequently, the broad-band UV photometry, perhaps more so than the narrow-band data, may average out astrophysically important wavelength-dependent effects due to convection andor photospheric granulation. Given this possible limitation of the broad-band *TD–1* data, as well as the generally low S/N of the narrow-band *TD–1* data, we have therefore undertaken a survey of high quality UV spectra of a sample of A– and early–F stars with the *IUE* spacecraft. The results of that effort are discussed in the next section. They are shown to confirm the conclusions we have reached here from the *TD–1* photometry.

3. *IUE* Spectroscopy of A–F Stars

3.1. Observations

The *IUE* spectra analyzed here consist of new observations as well as data from the public archives. All of the spectra were obtained with the short-wavelength prime (SWP) camera in its low dispersion mode, and were taken through the large science aperture. The spectral resolution is ~ 8Å. A full description of the *IUE* spacecraft and the performance of the telescope shortly after launch can be found in Boggess et al. (1978). Prior to our investigation, a number of *IUE* guest observers had obtained spectra of normal A– and F–type stars. Most of those images were heavily overexposed at the long wavelength end of the SWP camera (by factors of 5 or more) in order to enhance the detection of high temperature chromospheric and transition region lines at wavelengths shortward of 1700Å. However, a search of the archives yielded 32 spectra of 29 stars that were suitably exposed in the 1700–2000Å region of interest to us, and those spectra are included here in our survey of A–F stars. Nine of the same stars were reobserved by us.

The new observations consist of 64 spectra of 63 stars, the large majority of which stars are classified as spectroscopically normal. We excluded chemically peculiar (CP) Ap stars, but did include a few metallic line stars since Böhm-Vitense (1981b) found no difference between the *IUE* spectra of Am stars and those of normal A stars at wavelengths between 1400Å and 2500Å. Our analysis confirms this for the 1700–2000Å region (see also Praderie 1969).

Most of the new spectra were acquired during US#2 shifts and were occasionally subjected to high background radiation conditions. However, our exposure times were very

short, generally a few minutes or less (the longest being 8 minutes for 57 Tau), and so the quality of the spectrum was never adversely affected by the background radiation level. The integration times were generally chosen to achieve a peak exposure of 180–210 DN at wavelengths near 1900Å, to ensure that the exposure level would be close to the upper end of the linear section of the intensity transfer function (ITF). Except in five cases, the spectrum was either trailed, with a single pass of the star across the large aperture, or else multiply exposed at three standard offset positions within the large aperture, creating a "pseudo-trailed" spectrum. Two observations were taken as double exposures at different positions within the large aperture. Three others were single exposures made at the normal location and were subsequently processed as point source spectra.

The stars included in this survey, for which we have either new or archival spectra, are listed in Table 1. The table provides (V, $B-V$) on the Johnson system, plus $uvby\beta$ photometry gathered from the Hauck & Mermilliod (1990) catalog or from information cited in the SIMBAD database; estimates of the effective temperature, $T_{\rm eff}$, derived from $uvby\beta$ using the procedures described by Napiwotzki et al. (1993), which incorporate improvements to Moon & Dworetsky (1985); and comments that flag the known binaries and δ Scuti variables in our sample (Breger 1979, López de Coca et al. 1990). As was true of the *TD–1* sample discussed earlier, the $T_{\rm eff}$ values derived here show no evidence for a temperature plateau or for separate temperature sequences, and the rms spread of $\pm$120 K at a given $B-V$ or $b-y$ color index is not unexpected in light of either the calibration uncertainties cited by Napiwotzki et al. (1993) or the typical errors in $uvby\beta$ photometry quoted by Crawford & Perry (1966) and Crawford (1975).

Table 1 also lists the δc_1 and δm_1 indices for each star. As defined by Crawford (1975), these quantities assume β as the independent (temperature) variable: $\delta c_1(\beta) = c_1({\rm obs}) - c_1({\rm std})$ and $\delta m_1(\beta) = m_1({\rm Hyades}) - m_1({\rm obs})$. Although not strictly orthogonal, c_1 and m_1 serve as luminosity (surface gravity) and metallicity parameters, respectively (the m_1 index becomes progressively more sensitive to surface gravity at $B-V < 0.1$: Moon & Dworetsky 1985). The fundamental main sequence relations we adopt here are those established by Crawford & Perry (1966) and Crawford (1975, 1979), as updated and extended by Hilditch et al. (1983). In our analysis we explicitly allow for the fact that the m_1 relation is based on the Hyades Cluster, which is metal-rich compared to the Sun (Cayrel, Cayrel de Strobel, & Campbell 1985).

From each spectrum we measured an average flux at seven different wavelength positions from 1790Å to 1960Å. The last bin, centered on 1960Å, falls at the end of the SWP camera order. These mean fluxes were binned over wavelength intervals that were either 20Å or 40Å in width. The positions of the wavelength bins are illustrated in Figure

7, where they are drawn as horizontal lines beneath a spectrum of α Aquilae (Altair). The central wavelengths and widths of the bins were chosen to avoid known camera artifacts (the reseau marks) and also, to the extent possible, the strongest absorption features in the stellar spectrum.

The average fluxes measured in three representative wavelength bins are compiled in Table 2. We also give the corresponding Ultraviolet minus Visible colors, $[\lambda] = m(\lambda) - V$, where $m(\lambda)$ is the UV magnitude defined as before. The spectral images listed in Table 2 have all been extracted and calibrated with the NEWSIPS pipeline processing system (Nichols et al. 1994). As compared to the original IUESIPS processing scheme (Harris & Sonneborn 1987), NEWSIPS provides a much more optimal and uniform extraction, as well as automatic corrections for a variety of wavelength–, temperature–, and time–dependent instrumental effects. Before the NEWSIPS spectra were made available, however, we also measured the same images independently with the standard IUESIPS processing, except that we separately applied a number of corrections and adjustments. These were intended to compensate for: (1) the difference between the actual trail length and the nominal trail length assumed by IUESIPS (Garhart 1992a); (2) the quantization of the clock cycle of *IUE*'s on-board computer, which affects exposure segments shorter than 60^{s} (Harris & Sonneborn 1987, Oliversen 1991); (3) the temperature-sensitivity of the camera response, which was generally a $< 1\%$ effect (in no case was it $> 2\%$); and (4) the systematic on-orbit decay in the sensitivity of the SWP camera since the date *IUE* was launched (Bohlin & Grillmair 1988; Garhart 1992b). In the final step we used a table of sensitivity corrections kindly provided to us by R. Bohlin (1995, priv. comm.), which served to update the information published in Bohlin & Grillmair (1988). As described in the next paragraph, these IUESIPS corrected fluxes are on the whole 5–7% brighter than the corresponding NEWSIPS measurements. There is a similar zero point offset in the latest HST/FOS flux scale with respect to the NEWSIPS calibration (Colina & Bohlin 1994; Bohlin 1996), which suggests that our IUESIPS corrected fluxes are very nearly on the FOS scale.

To enable a conversion from the NEWSIPS flux scale to the IUESIPS scale, Table 2 includes a mean correction factor for each star, $C_{\rm IUE}$, which is an average over the full set of seven wavelength bands. Table 3 provides a mean correction factor for each wavelength bin, averaged over the entire set of stars. Both corrections are expressed in the sense of: the magnitudes by which the IUESIPS spectral fluxes are *brighter* than the NEWSIPS values listed in Table 2. As a general rule, the reader should be able to recover very nearly the actual IUESIPS measurements by combining the star-by-star and the bin-by-bin corrections. Because the NEWSIPS fluxes provide a marginally better fit to theoretical model atmosphere fluxes, as we will describe further below, there may be slight preference for the NEWSIPS fluxes over the IUESIPS ones. However, the choice of processing scheme

has little or no impact on the conclusions that we reach here (this will be made more evident, e.g., in Figure 14 below).

3.2. Color–Color Plots

A plot of $[\lambda]$, the UV color index from Table 2, versus the $B-V$ color index is shown for wavelengths of 1810Å and 1960Å in Figures 8a and 8b, respectively. Drawn for comparison in each panel is the main sequence relation predicted by ATLAS9 models (Kurucz 1993a,b, 1994), as well as a reddening line corresponding to a color excess $E(B-V) = 0.1$. The ATLAS models assume a surface gravity of $\log g = 4$, solar metal abundances, a microturbulent velocity $\xi_{\rm turb} = 2$ km s^{-1}, and, in the models that initiate convection (at $T_{\rm eff} < 9000$ K), a mixing-length to scale-height ratio equal to $l/H_{\rm p} = 1.25$. Also displayed are a pair of models at lower surface gravity, $\log g = 3.5$ and $\log g = 3$, and a pair with higher metal abundances, [M/H] = 0.3 and [M/H] = 0.5 (where the usual bracket notation specifies the logarithmic difference in M/H with respect to the Sun). The surface gravity that defines the main sequence relation is a compromise between a higher value that gives the best fit to the *IUE* photometry at 1960Å and a lower value required at 1810Å. In both panels, and for the other five wavelengths not shown here (the appearance of all these other plots is similar to Figure 8), the observations cluster around the model atmosphere curve. Neither panel of Figure 8 shows any sign of a temperature plateau or of two distinct temperature sequences. The vertical scatter in UV color around the model atmosphere relation is substantial, amounting to a range of ~ 0.65 mags at a given $B-V$. A scatter this large far exceeds the photometric errors of *IUE*, which are 3.5% or less in broad photometric bands (e.g., Garhart & Nichols 1995). We have verified this error estimate for our own particular wavelength bands by reprocessing more than 50 SWP low dispersion spectra of the *IUE* calibration standard BD+28°4211, which cover the same time period as our A–F star spectra. The resulting flux measurements are very nearly Gaussian distributed with a $\sigma = 0.035$ mags.

Given the slope of the normal reddening line, the better part of the scatter we observe among the A–F stars in Figure 8 cannot be due to interstellar extinction, since it is clear that differential reddening moves a star mostly parallel to the main sequence rather than across it. Furthermore, all of our stars are located close enough to the Sun that reddening effects are generally negligible, $\mathrm{E}(B-V) < 0.02$ (Perry & Johnston 1982). It is therefore difficult to see how a plausible amount of extinction could displace a star from a reasonable point of origin on the main sequence, somewhere to the left, to a location either well above or well below this curve. Some stars, e.g., β Pic, may suffer appreciable local or

circumstellar extinction (e.g., $A_v = 0.19$ for β Pic, according to Lanz, Heap, & Hubeny 1995), but their circumstellar particles are thought to be large enough that they should produce very little selective extinction, and hence should not displace a star off the main sequence relation in a color–color plot like Figure 8. Switching the abscissa from $B-V$ to an alternative photometric index, e.g., β or $b-y$, leads to some rearrangement of the points for individual stars (see Figure 9), but neither eliminates nor reduces the amount of scatter.

3.3. Instrumental Sources of the Scatter

Among possible instrumental origins of the scatter in Figures 8 and 9, we mention the following: (1) the observing and image processing mode (trailed, multiple-exposure, or point source), (2) the β angle of the observation, i.e., the orientation of the star with respect to the direction of the Sun at the time of observation, (3) the focus setting of the telescope, (4) the DN (or data number) exposure level or the exposure time of the spectral image, and (5) anomalies in the pointing and tracking of the telescope during an observation.

We consider first the observing and processing mode. Figure 10a plots the vertical deviation of the [1960Å] color of each star from the model atmosphere curve, $\delta 1960 \equiv [1960\text{Å}]_{obs} - [1960\text{Å}]_{model}$. The scatter does not appear to depend in any systematic fashion on the imaging mode, whether the image was trailed, pseudo-trailed (multiply exposed), or acquired in point source mode. At any given $B-V$, points for the different modes are intermixed. Likewise, in Figure 10b there is no correlation between $\delta 1960$ and the β angle of the observation over the full range of angles observed, from 40° up to 105°. This effectively rules out any significant contamination of our photometry by scattered solar radiation within the telescope. For the same reason, the spurious streak of light in the Fine Error Sensor (FES) formed by this light leak must never have compromised the guiding accuracy of our trailed spectra.

There is also no apparent relationship between the color deviations and the focus setting of the telescope (Figure 10c), the exposure level (DN) of the observation (Figure 10d), or the exposure time of the observation (Figure 10e). Residual non-linearities in the ITF therefore can be eliminated as a major cause of the scatter. Finally, we have confirmed by inspection of the observing log sheets that there were no significant problems with the tracking or pointing of the telescope in the course of any observation, except that of 49 UMa (image SWP46683), which the telescope operator noted as having a trail error of $\sim 4''$. The fluxes measured from this spectrum are not appreciably offset from the model atmosphere curve.

3.4. Intrinsic Causes of the Scatter: The Role of Stellar Rotation

If the onset of convection among the A–F stars causes the scatter observed in two–color plots such as Figure 8, then it is worthwhile inquiring whether this scatter correlates with other established proxies for convection, such as chromospheric emission in the C II 1335Å and H I Lyman α lines. We have demonstrated elsewhere that the strengths of these chromospheric features vary widely in A–F star spectra (Simon & Landsman 1991; Landsman & Simon 1993; Simon, Landsman, & Gilliland 1994), which suggests there is a broad range in the convection zone properties of these stars. However, the deviations in UV colors plotted in Figure 8 show no correlation with the normalized C II fluxes listed by Simon & Landsman (1991), and plots of $\delta 1810$ as well as $\delta 1960$ against X-ray emission (from Simon, Drake, & Kim 1995) are merely scatter diagrams. Thus, we find no direct link to connect the UV colors of the A–F stars with chromospheric and coronal proxies for convection.

The question of whether the stellar rotation speed regulates the onset of convection, as originally conceived by Böhm-Vitense & Canterna (1974) and BV82, is also susceptible to direct test. This involves a comparison of $\delta 1810$ and $\delta 1960$ with published values of $v \sin i$. Such a comparison indicates that the deviations in UV colors are uncorrelated with the stellar rotation rate, for stars inside the "A–star gap," $0.22 \leq B-V \leq 0.28$, and also for those outside it. Consider Figure 11. If stars within the gap are typically faster rotators, and if they define a low temperature radiative branch, characterized by generally larger UV color indices, then their points in this figure should fall systematically below those of the more slowly rotating stars that form the higher temperature convective plateau. Several of the gap stars, notably the δ Scuti variable 71 Tau, may follow this pattern, but there does not appear to be any distinct segregation of the points in either panel of Figure 11.

In addition, a number of stars inside the gap appear to be moderately slow rotators; some of them exhibit either chromospheric emission in C II or else have been detected in X rays (e.g., 22 Boo and ϵ Cep). If these stars are intrinsically slow rotators that have turned convective, the question is, why are they inside the gap instead of outside it, at $B-V > 0.28$? And if they are intrinsically rapid rotators seen nearly pole-on, why have they not remained radiative? Either way, they stand in conflict with the idea that rotation regulates the onset of convection among the A–F stars. Moreover, as noted previously by Simon, Drake, & Kim (1995), there are some rapidly rotating stars inside the gap showing both UV chromospheric emission and coronal X-ray emission, e.g., Altair and α Cep, which flatly contradict the idea that rapid rotation acts to suppress the onset of convection within the "A–star gap."

3.5. The Effect of Luminosity and Metallicity

In a sample of A–F stars chosen as broadly as ours, it would not be unduly surprising to find a range in the luminosity (=surface gravity) and chemical composition of the individual stars (cf. Berthet 1990, Edvardsson et al. 1993). Some impression of the importance of these parameters to the overall scatter in brightness at UV wavelengths can be derived from the model atmosphere fluxes plotted in Figure 8. With only a moderate range in the surface gravity, from $\log g = 4$ to $\log g = 3$, and in the metals to hydrogen ratio from solar to three times solar, that is, [M/H] = 0 to [M/H] = 0.5, the locus of model colors moves transverse to the standard main sequence and manages to cover virtually the entire range of UV and optical colors we have observed. This suggests that the observed scatter in the color–color plots might be accounted for by a modest spread in these properties throughout our sample of A and F stars. In fact, a plot of $\delta 1960$ shows strong trends with both the Strömgren luminosity index δc_1, and with the metallicity and line-blanketing index δm_1.

We have devised a method to adjust the observed colors of each star for potential gravity and metallicity effects, which makes use of the c_1 and m_1 indices. In effect, we attempt to restore each star back to the location it would have on the standard main sequence for solar abundances and a surface gravity of $\log g = 4$. Specifically, we define the correction for the UV color index at 1960Å (and similarly for all the other UV wavelengths) by a pair of linear relations,

$$\delta 1960 = \phi_1(T_{\rm eff} \mid \log g)\delta c_1,$$

$$\delta 1960 = \phi_2(T_{\rm eff} \mid M/H)\delta m_1,$$

where $\phi_{1,2}$ are polynomials in the β and/or $b-y$ index of integral and quarter-integral order. The coefficients in these polynomials were determined from a least-squares fit to the output of the ATLAS9 model atmosphere grid over the range $3 \leq \log g \leq 4$ and $-0.5 \leq [M/H] \leq 0.5$. The Strömgren indices, δc_1 and δm_1, are the observed values listed in Table 1. Similar expressions can be devised for the $B-V$ color index, but since the photometric indices of the Strömgren system are much more precisely defined and calibrated in terms of stellar properties, we prefer to work with $b-y$ instead. Thus,

$$\delta(b-y) = \psi_1(T_{\rm eff} \mid \log g)\delta c_1,$$

$$\delta(b-y) = \psi_2(T_{\rm eff} \mid M/H)\delta m_1.$$

Here, $\psi_{1,2}$ are also least-squares fitted polynomials in the β index and/or $b-y$. As noted earlier, the fiducial relation for m_1 is based on the Hyades Cluster, and so we adjust for the fact that $\delta m_1 = 0$ refers to a metal-rich composition (cf. Berthet 1990, Smalley & Dworetsky 1995).

A modified color–color plot using $b-y$ and UV colors corrected as just described is presented in Figure 12. To indicate that the colors have now been adjusted, we attach double primes to both indices, $(b-y)''$ and [1960Å]″. The result of having made these corrections is to produce a much tighter fit to the model atmosphere main sequence relation and to leave a smaller scatter in the observed color–color relation. In the process, these adjustments also eliminate the previously found correlated dependences of δ1960 on both δc_1 and δm_1.

With respect to the model atmosphere sequence, the rms scatter at 1960Å drops in half from ±0.25 mags to ±0.13 mags. Despite the reduced amount of scatter, the points still do not form a plateau or line up into two distinct sequences of stars, and furthermore a plot of the UV color deviations against rotation speed shows, as before, no obvious trend with $v \sin i$ (Figure 13). We note that some of the hottest stars in our sample, at $T_{\rm eff} > 8000$ K, are slightly displaced to more negative [1960Å]″ colors with respect to the radiative ATLAS9 models, but the difference is at most 0.2 mags. Except for this slight offset in the NEWSIPS colors, we can point to no other systematic trends in the scatter in our color–color plots following the luminosity and abundance adjustments we have made. If, for example, we reconsider the question of instrumental scatter raised in Section 3.3, no correlation emerges in the adjusted data with respect to (1) the imaging mode, (2) the β angle of the observation, (3) the camera focus setting, or (4) the DN exposure level of the spectrum. Figure 10 offers the details.

3.6. Microturbulence

Our use of ATLAS models to calibrate δm_1 against [M/H] makes the implicit assumption that the Strömgren index is a surrogate for the chemical composition of a star. The fact that the adjusted colors we derive show less scatter, rather than more, tends to validate this hypothesis. However, the effects of a range in metallicity on model atmosphere fluxes can be mimicked by a spread in microturbulent velocity (for a related discussion, refer to Smalley 1993). An increase in the overall metal abundance by a factor of 2 above solar raises the predicted m_1 index by nearly 0.02 mags. An increase in $\xi_{\rm turb}$ from 2 km s^{-1}, the nominal value we have adopted here, to 4 km s^{-1} does precisely the same. At wavelengths in the *IUE* range, metallicity has the stronger influence of the two. For a factor of two higher metallicity, [1960Å] changes by 0.4 mags; but doubling the value of $\xi_{\rm turb}$ from 2 km s^{-1} to 4 km s^{-1} produces only a 0.1 mag change. Consequently, if the ~ 0.65 mag scatter observed in the colors of the A stars is due to the influence of microturbulence alone, then the range in $\xi_{\rm turb}$ in our *IUE* sample would have to go well outside the limits of 2–4 km s^{-1}

that have been established from studies of line profiles and abundance analyses for stars of this class (e.g., Lane & Lester 1987; Lemke 1989; Coupry & Burkhart 1992).

Some of the residual scatter of ±0.13 mags that remains in color–color plots like Figure 12 could be associated with a normal spread in the individual values of $\xi_{\rm turb}$, but to prove this would require velocity estimates for many more stars in our *IUE* sample than are now available. There is some overlap between our sample and the F-star sample of Balachandran (1990). Her study provides microturbulent velocities (albeit only indirect estimates) for a half-dozen stars in common, including HR 2740, which has the most extreme color deviation $\delta 1960''$ of any star that we observed. The microturbulent velocity assigned by Balachandran to HR 2740 is unexceptional, $\xi_{\rm turb} = 1.9$ km s^{-1}. The values she reports for the remaining stars are also in the range of 1.8 to 2.1 km s^{-1}, being equally unremarkable. Five other stars in our survey were analyzed by Russell (1995), who obtained microturbulent velocities $\xi_{\rm turb} \approx 2.5$ km s^{-1} for each of them; the range in $\delta 1960''$ is 0.18 mags. On the basis of these two studies, then, we would be inclined to say that microturbulence likely has only a minimal impact on the spread in UV colors of the A–F stars, but at this stage our assessment is by no means definitive.

3.7. Intrinsic Variability

Unresolved binaries have been suggested as a major source of "noise" in *uvbyβ* photometry (Crawford & Perry 1966). When it comes comes to explaining the scatter in the UV colors of A stars, however, binary status seems to matter very little. There is no difference in the range of $\delta 1960''$ among the single stars and those classified as either spectroscopic or wide doubles (see Figure 13b). Also, the rms scatter for the binaries, ±0.12 mags after the luminosity and metallicity adjustments described in Section 3.5, is very close to the rms scatter of ±0.13 mags in the sample as a whole.

Similarly, the behavior of the known δ Sct pulsators in our sample is indistinguishable from that of the non-δ Sct stars. The rms deviation in the adjusted colors of the variables, ±0.12 mags, is practically the same as that of the full sample. Moreover, a histogram of the individual deviations, $\delta 1960''$, shows a similar, if not slightly narrower, spread for the variable stars than for the non-variables (Figure 14). The largest amplitude in V among all the δ Sct stars we observed is 0.05 mags for υ UMa (López de Coca et al. 1990). For the remainder, the amplitudes at V are typically ≤ 0.02 mags. Three of the δ Sct stars we observed had spectra in the archives: LW Vel (HR 4017) was virtually the same in 1800–2000Å brightness in its archival spectrum as when we observed it (to within 4%); ρ Tau was 10% brighter in our spectrum; and 71 Tau was 20% brighter in our observation

than it was five months later when Monier & Kreidl (1994) observed it. During the single 8-hour *IUE* shift that 71 Tau was observed by those authors, no variations were seen in the UV brightness of this star on a timescale comparable with its ∼3.9-hour stellar pulsation period.[3]

In the course of our survey, we also observed HD 224638, a member of the γ Doradus class of non-radial g-mode pulsators (Balona et al. 1994; Mantegazza et al. 1994). The fluxes measured from the *IUE* spectrum of HD 224638 show only a small departure of –0.05 mags from the standard model atmosphere color–color sequence.

The majority of the non-variable stars observed with *IUE* lie within the boundaries of the well-known pulsation instability strip (e.g., Breger 1979). Presumably, under the right circumstances, these stars might also be subject to pulsational instability. However, if their pulsation amplitudes were small enough, photometric variability might be noticeable only at UV wavelengths, where the stellar spectral energy distribution is several times more sensitive to $T_{\rm eff}$ than it is at visible wavelengths. If we assume for discussion that the residual rms scatter of ± 0.13 mags in the UV colors is the result of intrinsic variability, the implied temperature variation amounts to $\Delta T_{\rm eff} = \pm 100$ K. The corresponding brightness change expected at optical wavelengths for this $\Delta T_{\rm eff}$ is $\Delta V = \pm 0.07$ mags. Variability this pronounced would certainly have been noticed in time-series $uvby\beta$ photometry, which routinely achieves an accuracy of just a few millimags. On the other hand, variability at half that amplitude, $\Delta V \approx \pm 0.03$ mags, might well have been missed in isolated photometry taken with no forethought of variability, especially if the changes happened to be irregular or multiperiodic in character.

Twelve of our stars had repeat measurements with *IUE* that can be examined for ultraviolet variability. Just two stars, 71 Tau and ρ Tau, both δ Sct variables, showed clear signs of variability in excess of the mean photometric errors of ± 0.04 mags. In the case of 71 Tau, the timescale of the UV variability is unknown but the changes appear to be unrelated to the short-period δ Sct pulsation because of (a) the lack of variability reported in the prior study of Monier & Kreidl (1994), and (b) the very improbable 10:1 UV-to-optical amplitude ratio implied by the color deviations of the *IUE* archival spectra of this star. Thus, while we cannot show from the observational evidence, such as it is, that intrinsic variability makes a significant contribution to the scatter in our two color plots, it may be premature to dismiss this possibility until the variations of a star like 71 Tau are better understood and the full range of its pulsational behavior has been more thoroughly

[3] 71 Tau lies below the standard sequence in our color–color plots. It has a late-type companion and, given its $B-V$ color, might have been expected to appear comparatively brighter in the UV, not fainter.

explored.

4. Conclusions

We have used broad-band *TD–1* photometry and high quality spectra from the *IUE* spacecraft to explore the possible effects of subsurface convection on the spectral energy distributions of normal, main sequence A and F stars. In particular, we have examined a proposal originally offered by Böhm-Vitense, that the onset of convection among the A–F stars may lead to the formation of two distinct temperature sequences, one comprised of the convective stars, the other consisting of the radiative stars. We see no evidence for any temperature bifurcation in the two samples of stars we have studied with *TD–1* and *IUE*. Given the very small internal photometric errors of the *IUE* spectrophotometry, typically $\pm 3.5\%$ or better in observed flux, or equivalently ± 25 K in stellar effective temperature, we should have easily seen and thus confirmed a systematic separation in $T_{\rm eff}$ as large as the 500 K difference claimed by Böhm-Vitense from her study of the narrow-band *TD–1* photometry (BV82).

On the other hand, we do find a considerable dispersion in the UV colors observed with *IUE*, up to 0.6 mags or more at a given $B-V$ color index. A number of possible extrinsic and intrinsic explanations for the scatter can be eliminated: various instrumental and/or image processing effects, interstellar or circumstellar extinction, binarity, a spread in the rotation rates of individual stars, or the onset of convective activity in the form of hot chromospheres and coronas. The most plausible cause, we find, is a range in the surface gravities and metallicities of the stars in our survey. Through a comparison with ATLAS9 model atmosphere fluxes, we can account for at least 0.4 mags of the scatter with a 1 dex spread in gravity and a 0.5 dex spread in the metals-to-hydrogen ratio. Another 0.1–0.2 mags may arise out of a normal dispersion of a few km s^{-1} in atmospheric microturbulence (through its influence on the degree of line blanketing). A similar contribution may come from photometric variability if the stars in our survey prove to be marginally stable against pulsation. Evidence for this is very weak.

A more plausible interpretation for the residual UV scatter of ~ 0.25 mags can be found in the empirical relation between metal abundance and the Strömgren δm_1 index, which forms the basis for the technique we have used to adjust the *IUE* colors for differing amounts of spectral line blanketing. According to Figure 6 of Berthet (1990), among the A and F stars there is a spread of 0.4 dex or more in the Fe/H ratio at a fixed value of δm_1. Very nearly the same spread is present in the more homogeneous dataset of Smalley (1993: see his Figure 3). A dispersion in [M/H] of this order overlaps the entire

range of scatter shown here in Figure 8, and moreover is fully consistent with the size of the discrepancies between the spectroscopic and photometric determinations of [Fe/H] obtained by Balachandran (1990) for her set of F stars. In our analysis we also make a common simplifying assumption, which may not be truly justified, viz., that the chemical abundances of the elements responsible for most of the UV line blanketing scale together. In the 1700–2000 Å region, Fe II and Si I both have a number of strong absorption lines in A–F star spectra. In the spectroscopic survey of nearby F–G field stars conducted by Edvardsson et al. (1993), these two elements vary by 0.2 dex or more in relative abundance from one star to the next. If this is true as well among the A–F stars, then a single photometric index like δm_1 can provide only a first-order correction for UV line blanketing; more detailed abundance analyses may therefore be required in order to lower the scatter in our color–color diagrams below the current residual level of ~ 0.25 mags.

Although we find in our study no evidence for any gross changes in the UV colors of A and F stars that might be associated with the onset of subsurface convection, the search for more subtle signatures in the photospheric lines and spectral energy distributions of these stars nevertheless remains a worthwhile goal. In particular, the correlation of photospheric features with established chromospheric and coronal proxies for convection would provide valuable constraints on both the proper model of convection, as well as the source of the non-radiative heating. However, as we have shown in this paper, the detection of a photospheric signature of convection will first require a more detailed analysis of the effects of metallicity, gravity, and microtubulence — and possibly variability — on the spectra of the A and F stars.

We thank Dr. Y. Kondo and the staff of the *IUE* observatory for their assistance in the acquisition and reduction of these data. This research has made use of the SIMBAD database, operated by the Centre de Données astronomiques de Strasbourg. The authors thank R. L. Kurucz for discussions and assistance with the ATLAS model atmospheres, and R. C. Bohlin for providing us with updates to the *IUE* camera sensitivity function.

REFERENCES

Balachandran, S. 1990, ApJ, 354, 310

Balona, L. A., Krisciunas, K., & Cousins, A. W. J. 1994, MNRAS, 270, 905

Berthet, S. 1990, A&A, 236, 440

Boggess, A. 1978, Nature, 275, 2

Bohlin, R. C., & Grillmair, C. J. 1988, ApJS, 68, 487

Bohlin, R. C., & Holm, A. V. 1984, NASA IUE Newsletter, 24, 74

Bohlin, R. C. 1996, AJ, 111, 1743

Böhm-Vitense, E. 1970a, A&A, 8, 299

——. 1970b, A&A, 8, 283

——. 1978, A&A, 223, 509

——. 1981a, ARAA, 19, 295

——. 1981b, ApJ, 244, 938

——. 1982, ApJ, 255, 191 (BV82)

Böhm-Vitense, E., & Canterna, R. 1974, ApJ, 194, 629

Breger, M. 1979, PASP, 91, 5

Cayrel, R., Cayrel de Strobel, G., & Campbell, B. 1985, A&A, 146, 249

Colina, L., & Bohlin, R. C. 1994, FOS Instrument Science Report on Standard Calibration Sources CAL/SCS-003 (STScI internal document)

Coupry, M. F., & Burkhart, C. 1992, A&AS, 95, 41

Crawford, D. L. 1975, AJ, 80, 955

——. 1979, AJ, 84, 1858

Crawford, D. L., & Perry, C. L. 1966, AJ, 71, 206

Dravins, D. 1990, A&A, 228, 218

Edvardsson, B., Andersen, J., Gustafsson, B., Lambert, D. L., Nissen, P. E., & Tomkin, J. 1993, A&A, 275, 101

Garhart, M. P. 1992a, *IUE* Newsletter No. 48, p. 88

——. 1992b, *IUE* Newsletter No. 48, p. 98

Garhart, M. P., & Nichols, J. S. 1995, *IUE* Newsletter No. 55, p. 39

Gilliland, R. L. 1986, ApJ, 300, 339

Gray, D. F. 1989, PASP, 101, 832

Harris, A. W., & Sonneborn, G. 1987, in "Exploring the Universe with the *IUE* Satellite," ed. Y. Kondo et al. (Dordrecht: Reidel), p. 729

Harris, G. L. H., FitzGerald, M. P. V., Mehta, S., & Reed. B. C. 1993, AJ, 106, 1533

Hauck, B., & Mermilliod, M. 1990, A&AS, 86, 107

Hilditch, R. W., Hill, G., & Barnes, J. V. 1983, MNRAS, 204, 241

Hoffleit, D., & Jaschek, C. 1982, The Bright Star Catalogue (New Haven: Yale University Observatory)

Houk, N., & Fesen, R. 1978, in "IAU Symposium 80, The HR Diagram", ed. A. G. Davis Philip & D. S. Hayes (Boston: Reidel), p 91

Jamar, C., Macau-Hercot, D., Monfils, A., Thompson, G. I., Houziaux, L., & Wilson, R. 1976, *Ultraviolet Bright-Star Spectrophotometric Catalogue* (Paris: ESA), SR-27

Kjeldsen, H., & Frandsen, S. 1991, A&AS, 87, 119

Kurucz, R. L. 1993a, in "Peculiar Versus Normal Phenomena in A–Type and Related Stars," ed. M. M. Dworetsky, F. Castelli, & R. Faraggiana, A.S.P. Conf., 44, 87

Kurucz, R. L. 1993b, "ATLAS9 Stellar Atmosphere Programs and 2 km s^{-1} Grid," SAO CD-ROM No. 13 © Smithsonian Astrophysical Observatory

Kurucz, R. L. 1994, "Solar Abundance Model Atmospheres for 0, 1, 2, 4, 8 km s^{-1}," SAO CD-ROM No. 19 © Smithsonian Astrophysical Observatory

Landsman, W., & Simon, T. 1993, ApJ, 408, 305

Lane, M. C., & Lester, J. B. 1987, ApJS, 65, 137

Lanz, T., Heap, S. R., & Hubeny, I. 1995, ApJL, 447, L41

Lemke, M. 1989, A&A, 225, 125

López de Coca, P., Rolland, A., Rodríguez, E., & Garrido, R. 1990, A&AS, 83, 51

Macau-Hercot, D., Jamar, C., Monfils, A., Thompson, G. I., Houziaux, L., & Wilson, R. 1978, *Suppl. Ultraviolet Bright-Star Spectrophotometric Catalogue* (Paris: ESA), SR-28

Malaise, F., Gros, M., & Macau, D. 1974, A&A, 33, 79

Mantegazza, L., Poretti, E., & Zerbi, F. M. 1994, MNRAS, 270, 439

Monier, R., & Kreidl, T. J. 1994, A&A, 284, 210

Moon, T. T., & Dworetsky, M. M. 1985, MNRAS, 217, 305

Napiwotzki, R., Schönberner, D., & Wenske, V. 1993, A&A, 268, 653

Nelson, G. D. 1980, ApJ, 238, 659

Nichols, J. S., Garhart, M. P., De La Penã, M. D., & Levay, K. L. 1994, *IUE* Newsletter No. 53

Nordlund, Å., & Dravins, D. 1990, A&A, 228, 155

Oliversen, N. 1991, *IUE* Newsletter No. 45, p. 56

Perry, C. L., & Johnston, L. 1982, ApJS, 50, 451

Praderie, F. 1969, in "Theory and Observation of Normal Stellar Atmospheres," ed. O. Gingerich (Cambridge, MA: The M.I.T. Press), p. 215

Russell, S. C. 1995, ApJ, 451, 747

Saxner, M., & Hammarbäck, G. 1985, A&A, 151, 372

Simon, T., Drake, S. A., & Kim, P. D. 1995, AJ, 107, 1034

Simon, T., & Landsman, W. 1991, ApJ, 380, 200

Simon, T., Landsman, W. B., & Gilliland, R. L. 1994, ApJ, 428, 319

Smalley, B., & Dworetsky, M. M. 1993, A&A, 271, 515

——. 1995, A&A, 293, 446

Thompson, G. I., Nandy, K., Jamar, D., Monfils, A., Houziaux, L., Carnochan, D. J., & Wilson, R. 1978, *Catalogue of Stellar Ultraviolet Fluxes*, U.K. Science Research Council.

van 't Veer-Menneret, C., Faraggiana, R., & Burkhart, C. 1980, A&A, 92, 13

van 't Veer-Menneret, C., & Mégessier, C. 1996, A&A, 309, 879

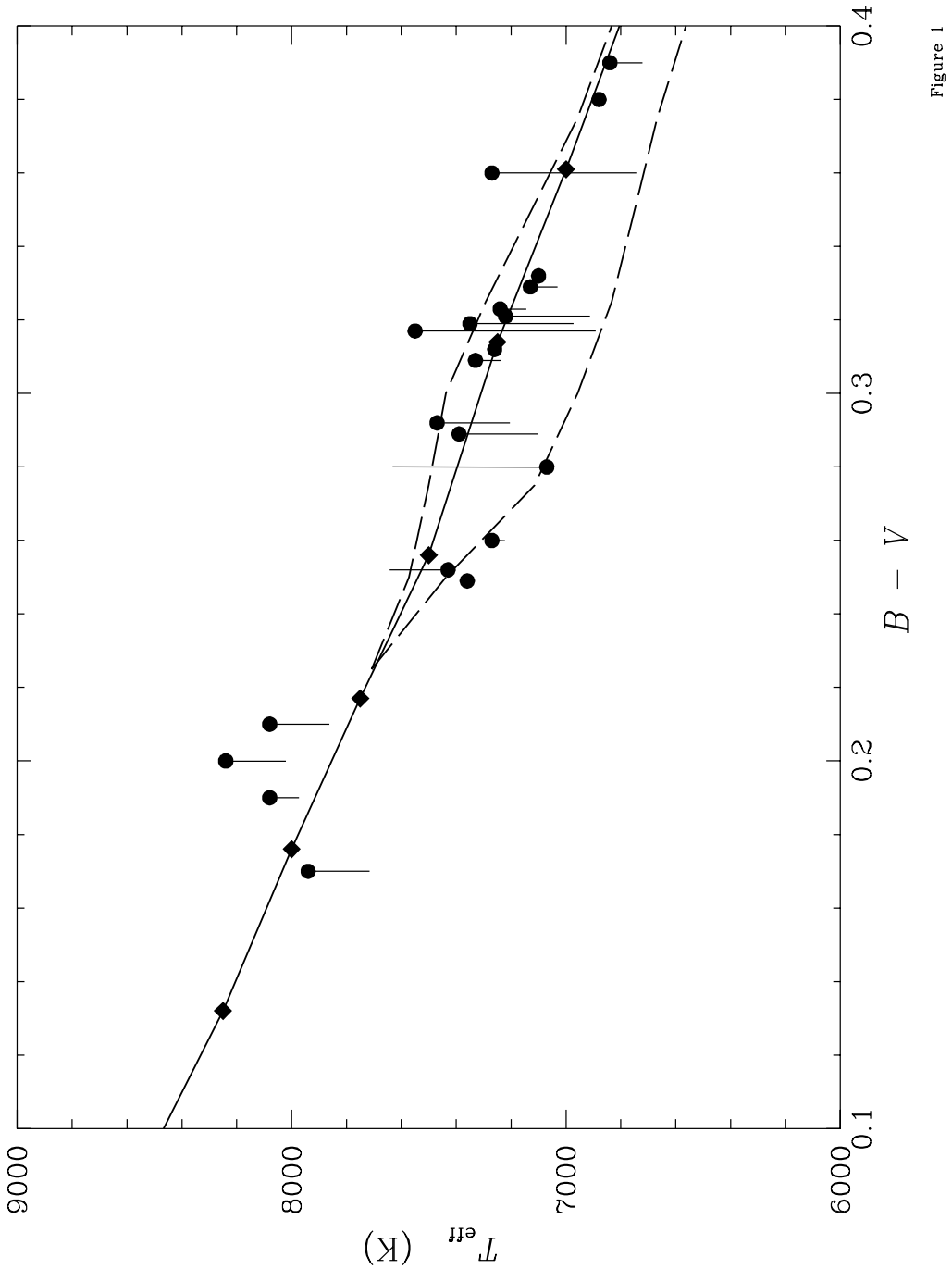

Fig. 1.— Effective temperature versus $B-V$ color for main sequence A–F stars. The filled circles are estimates derived from *TD–1* photometry by Böhm-Vitense (1982, Table 3), while the vertical lines are the revisions we obtain by applying the method of Napiwotzki et al. (1993) to *uvbyβ* photometry. The diamonds connected by solid lines are ATLAS model atmospheres (Kurucz 1993a). The dashed lines denote the upper convective branch and lower radiative branch of Böhm-Vitense (1982), as transcribed from Figure 7 of that paper, except that we omit the evolved giants and bright giants that were included in the original figure.

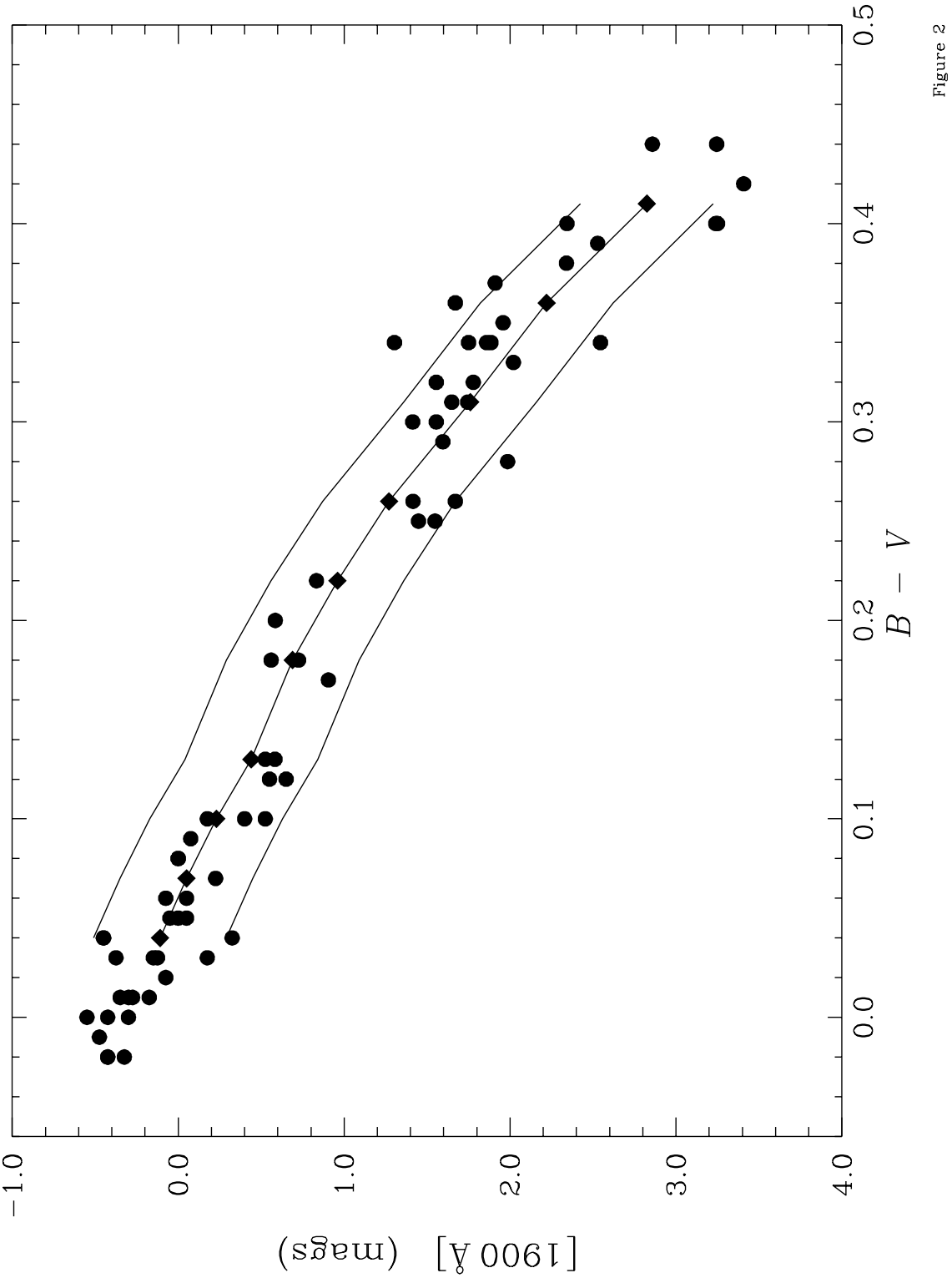

Fig. 2.— Narrow-band *TD–1* photometry for A–F stars (*filled circles*) and model atmosphere fluxes (*filled diamonds*). $m1900$Å) is the narrow-band *TD–1* magnitude. Plotted here are the stars that appear in Tables 1 and 2 of Böhm-Vitense (1982). The solid lines drawn parallel to the model atmosphere curve are offset vertically by ±0.4 mags.

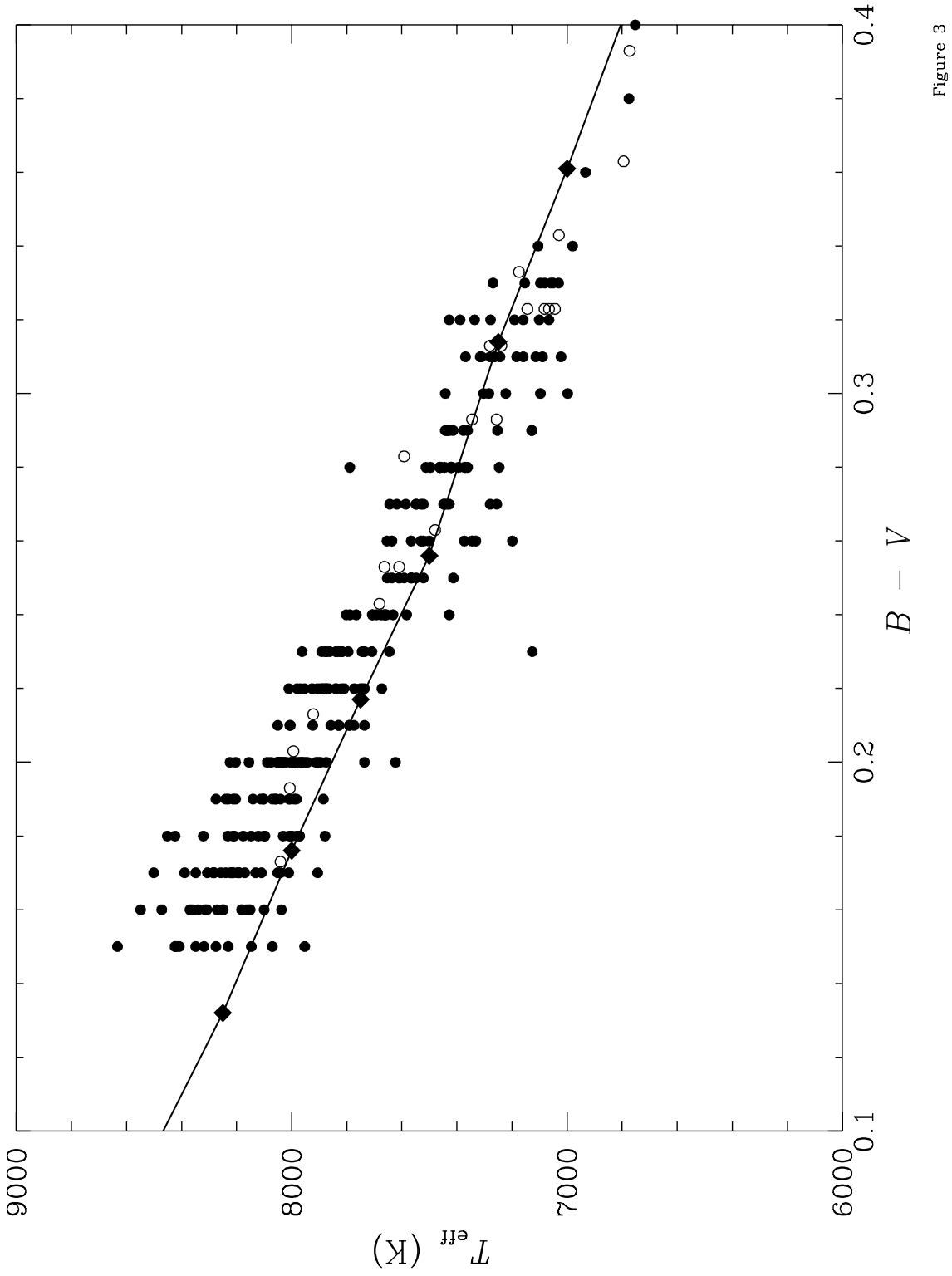

Fig. 3.— Effective temperatures from Strömgren photometry for A–F stars with *TD–1* broad-band photometry. Chemically normal stars are shown by filled circles, stars from Böhm-Vitnese (1982) as open circles (offset slightly in $B-V$ color for clarity).

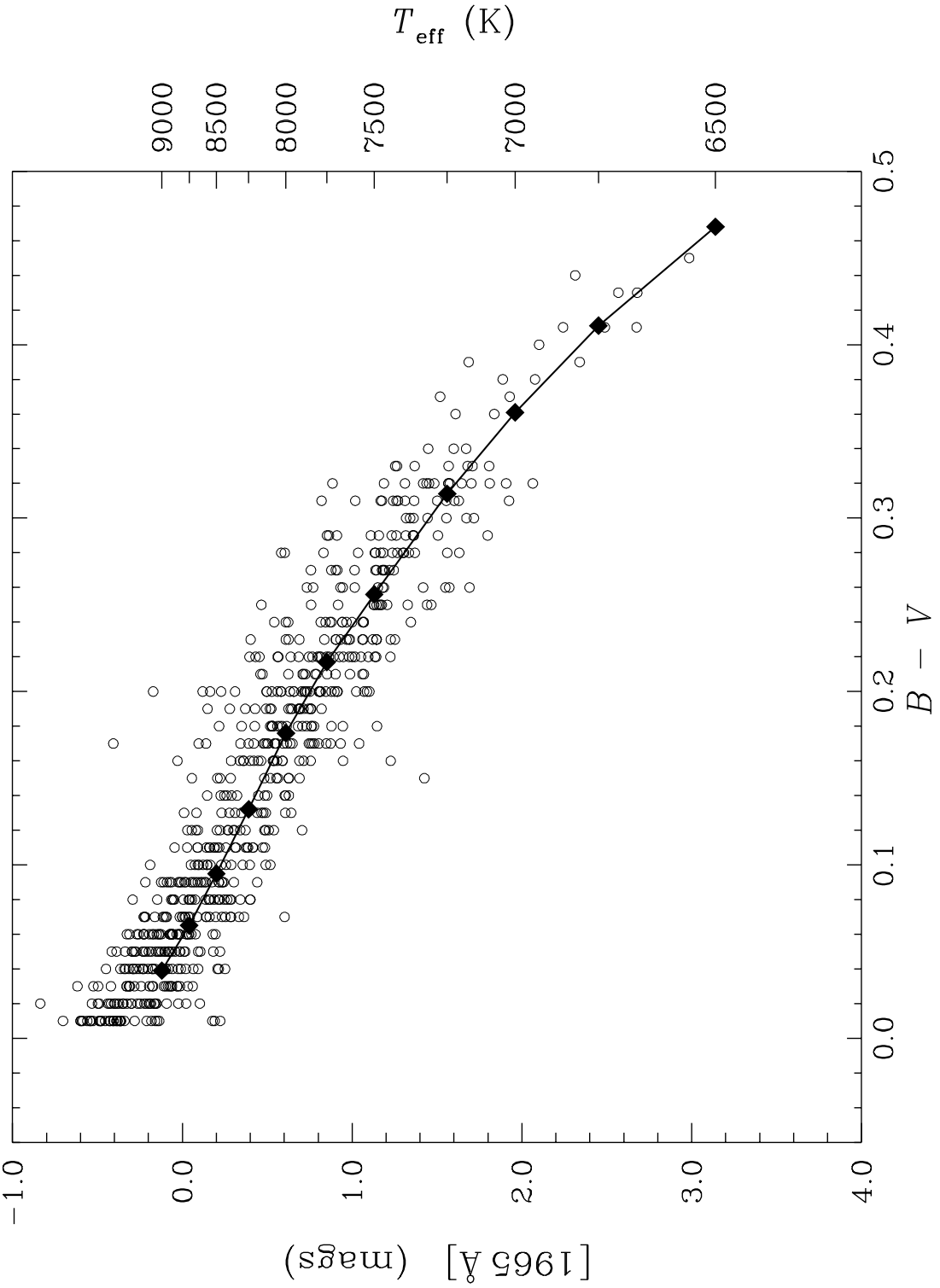

Figure 4

Fig. 4.— Broad-band ultraviolet (1965Å) minus V color for *TD–1* stars, plotted versus $B-V$ color. The diamond symbols denote ATLAS9 models.

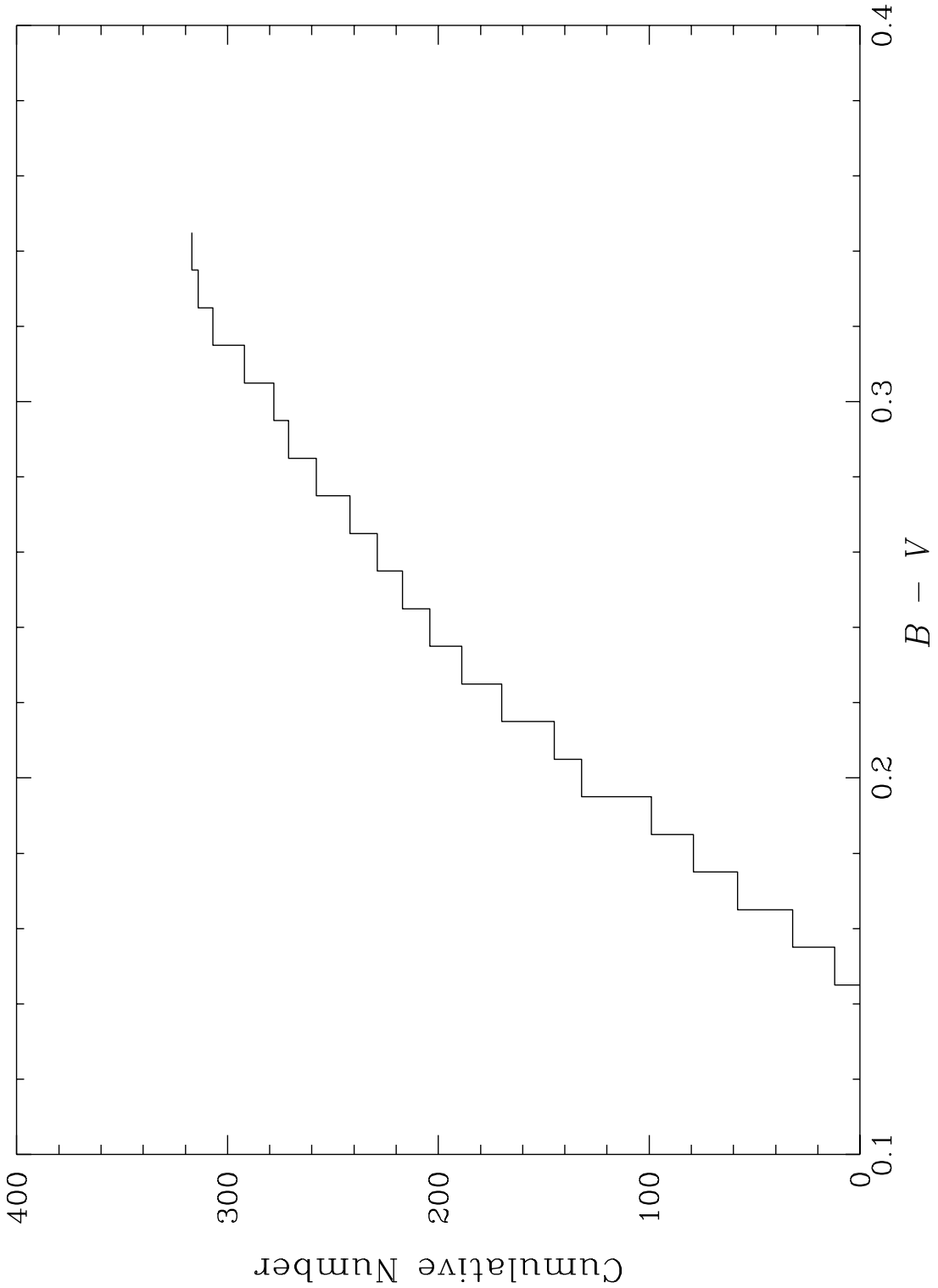

Fig. 5.— Cumulative count of *TD–1* stars with colors in the range $0.15 \leq B-V \leq 0.33$. An absence of stars in the vicinity of the A–star gap, $0.22 \leq B-V \leq 0.28$ would be signified by a horizontal plateau in the cumulative distribution function. We see no evidence in this range of colors for a gap in our *TD–1* sample.

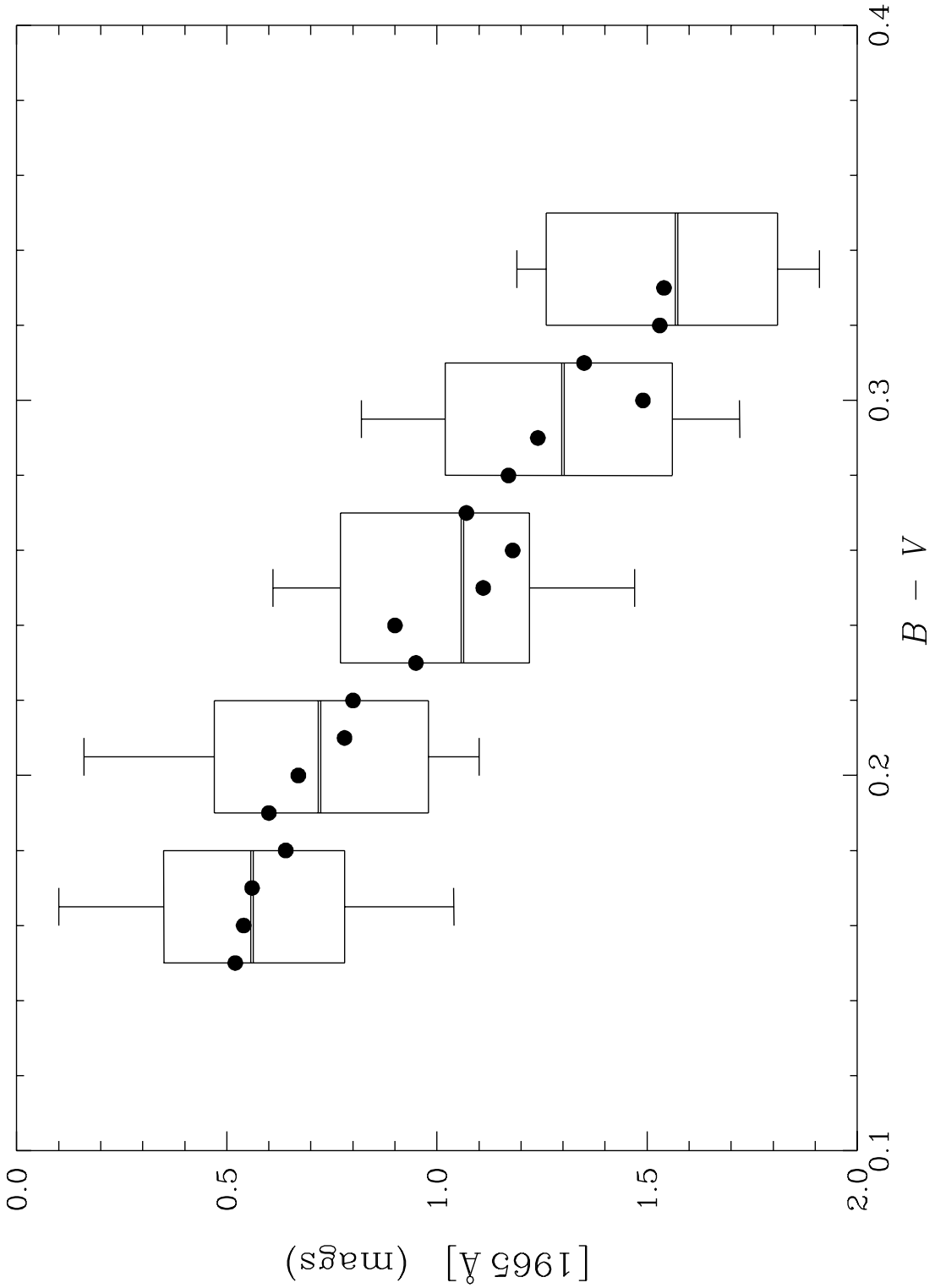

Figure 6

Fig. 6.— The distribution function of broad-band 1965Å *TD–1* colors of main sequence stars for five $B-V$ color bins. The percentile levels shown by the box plots are at: 95% and 5% (*vertical bars*), 84% and 16% (*upper and lower edges of the box*), and 50% (*double bar within the box*). Also shown is the mean $B-V$ color, computed for 0.01 mag intervals in $B-V$.

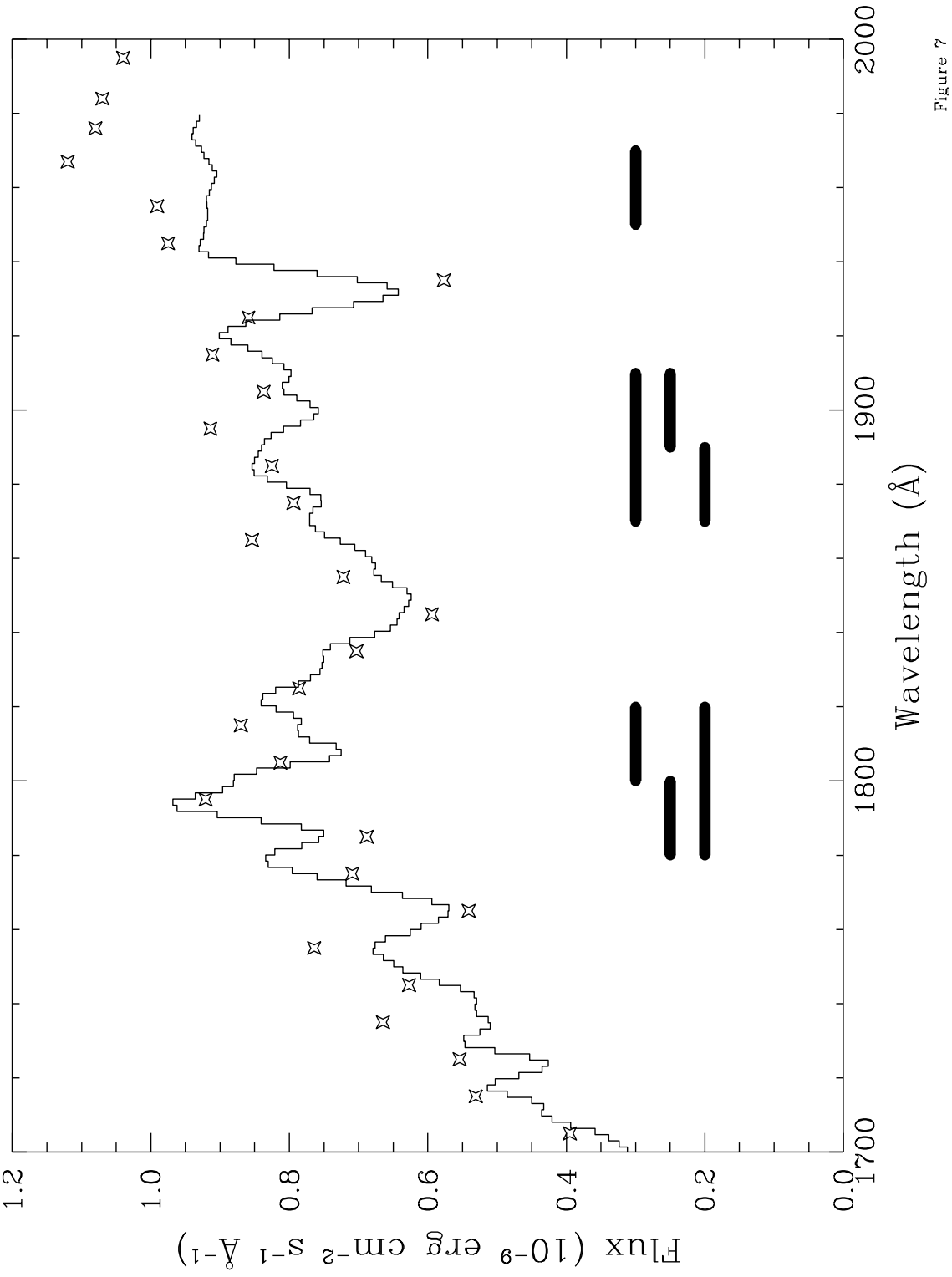

Fig. 7.— Trailed *IUE* low dispersion spectrum of α Aql (SWP 45755, effective exposure time of 3.4 s), and for comparison the UV flux distribution predicted by an ATLAS9 model having $T_{\rm eff} = 7900$ K and $\log g = 4$. The horizontal lines drawn below the spectrum show the wavelength bins for which we have measured average fluxes for each star.

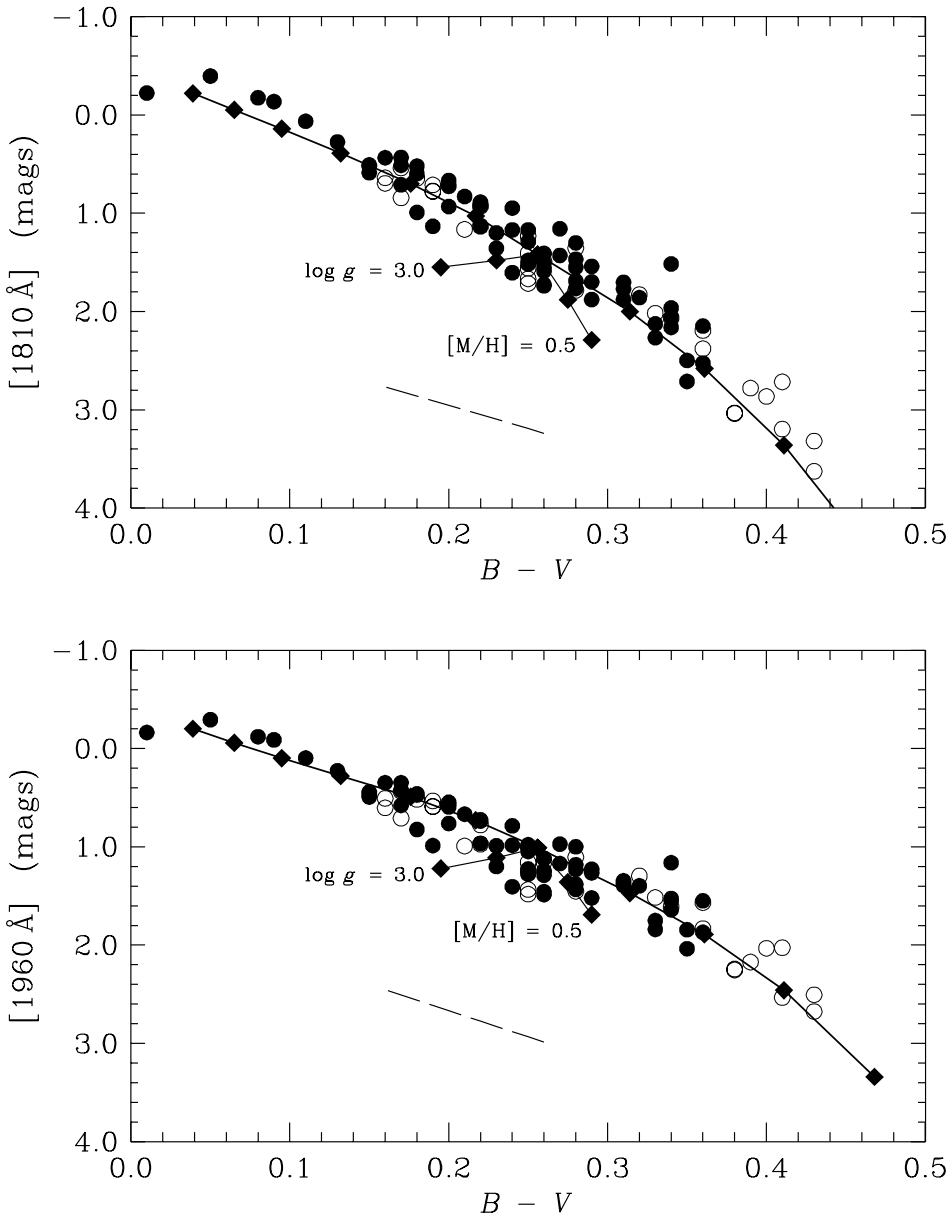

Figure 8

Fig. 8.— Color–color plots for stars observed with *IUE*: (a) for a wavelength of 1810Å, (b) for a wavelength of 1960Å. *Filled circles*: UV spectra obtained in our guest observer program. *Open circles*: archival data. The filled diamonds are ATLAS9 models, those extending below and to the left of the main sequence illustrating the effects of a lower surface gravity (for models with $T_{\rm eff} = 7500$ K, solar abundances, and $\log g = 3.5$ and 3.0), and those to the right showing the effects of an increase in the heavy element abundances (for [M/H] = 0.3 and 0.5). The dashed line is a normal interstellar reddening line for a color excess of E($B-V$) = 0.1 mags.

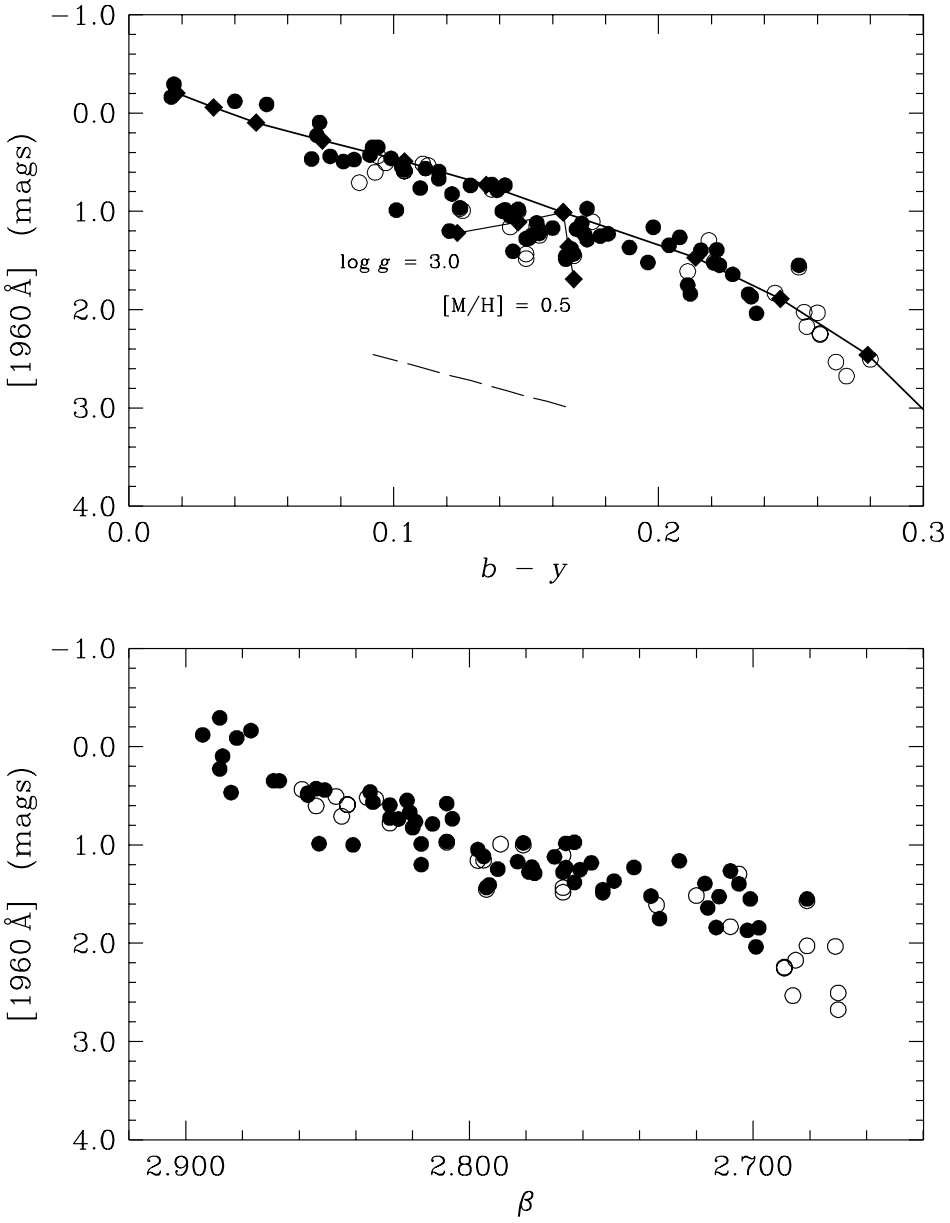

Figure 9

Fig. 9.— Two–color plot with $b-y$ as the abscissa (*top panel*) and the Strömgren Hβ index, β, as the abscissa (*bottom panel*). The symbols are the same as in Fig. 8. The $B-V$ boundaries of the A–star gap correspond approximately to $0.12 \leq b-y \leq 0.21$.

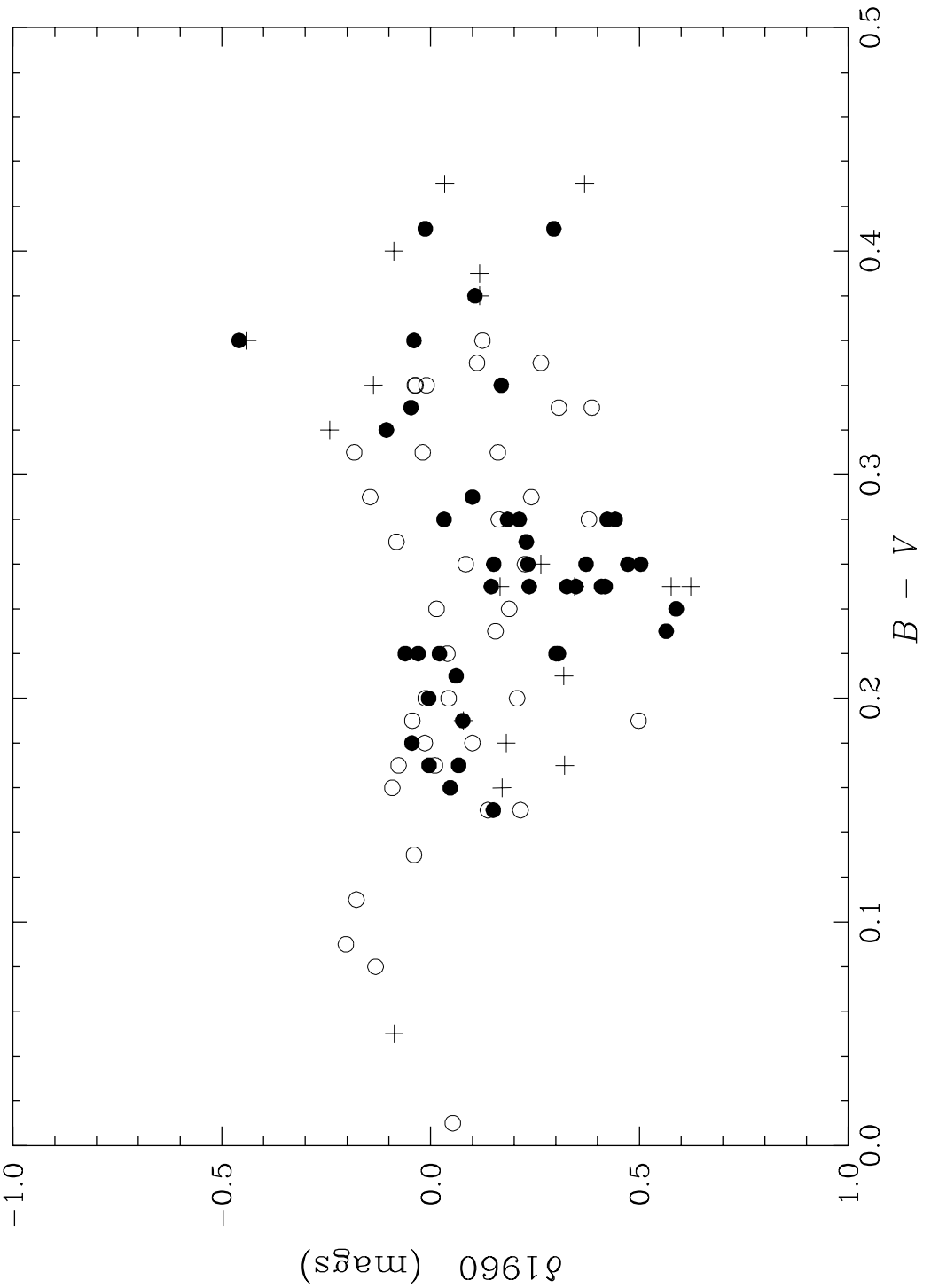

Fig. 10.— (a) The deviations in UV color as a function of imaging mode (*plus signs*: point source, *filled circles*: trailed, *open circles*: multiple exposure). (b) Deviations versus β angle of the observations (*filled circles*: original colors, *open circles*: luminosity– and metallicity–corrected colors). (c) Same as (b) for the *IUE* SWP camera focus setting. (d) Same as (b) for the maximum DN exposure level in the spectral image. (e) Same as (b) for the exposure time of the image.

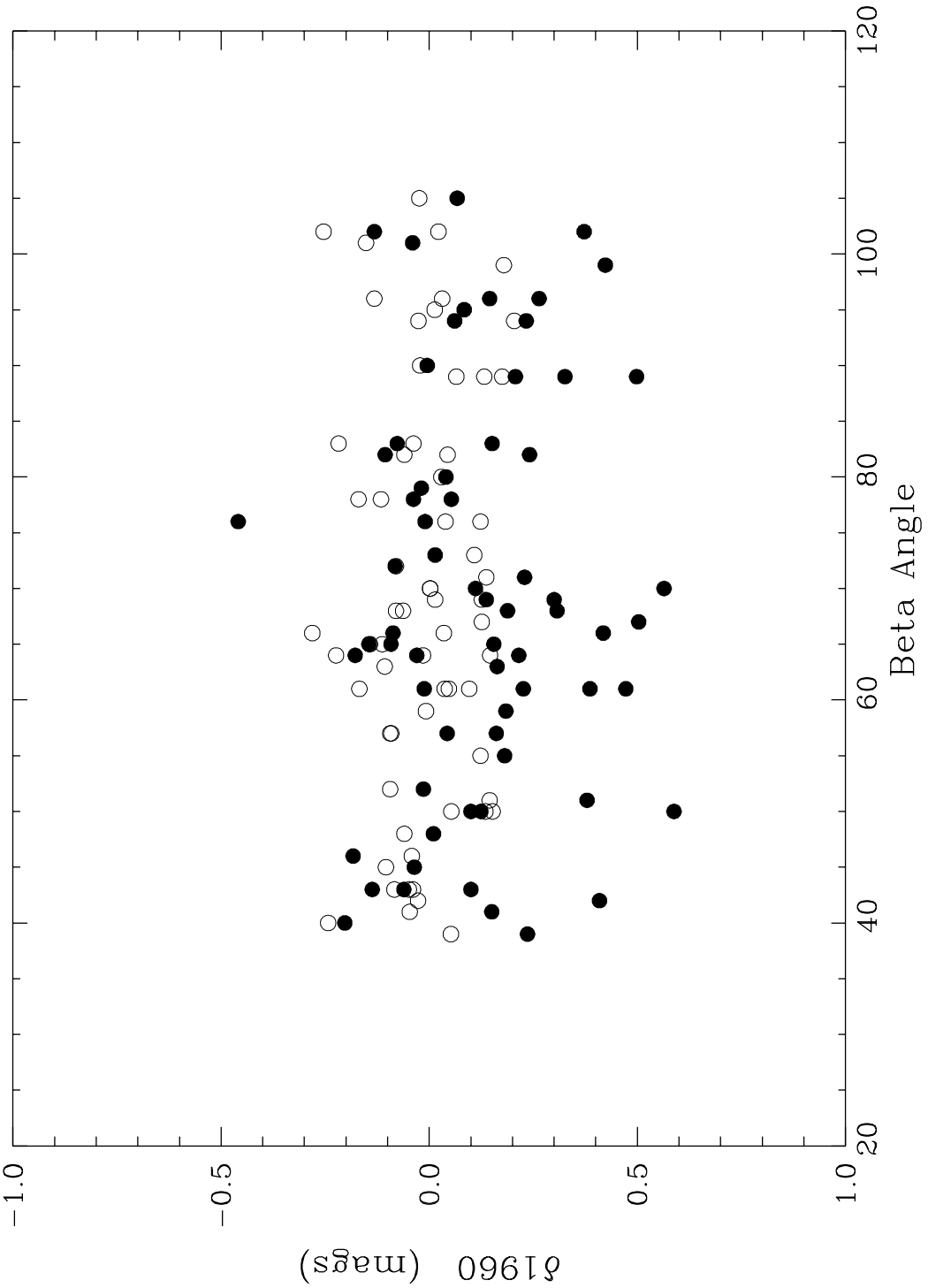

Figure 10b

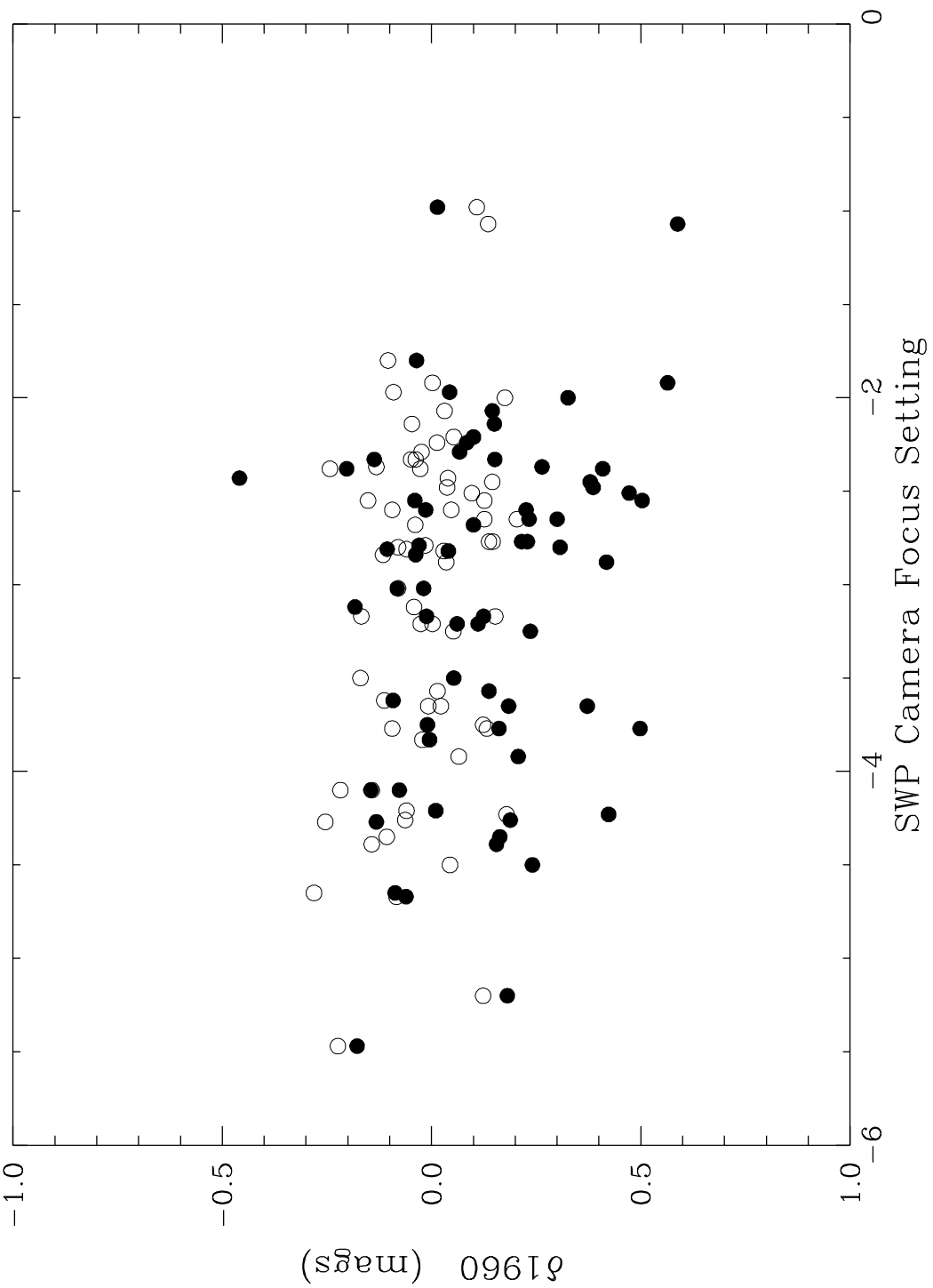

Figure 10c

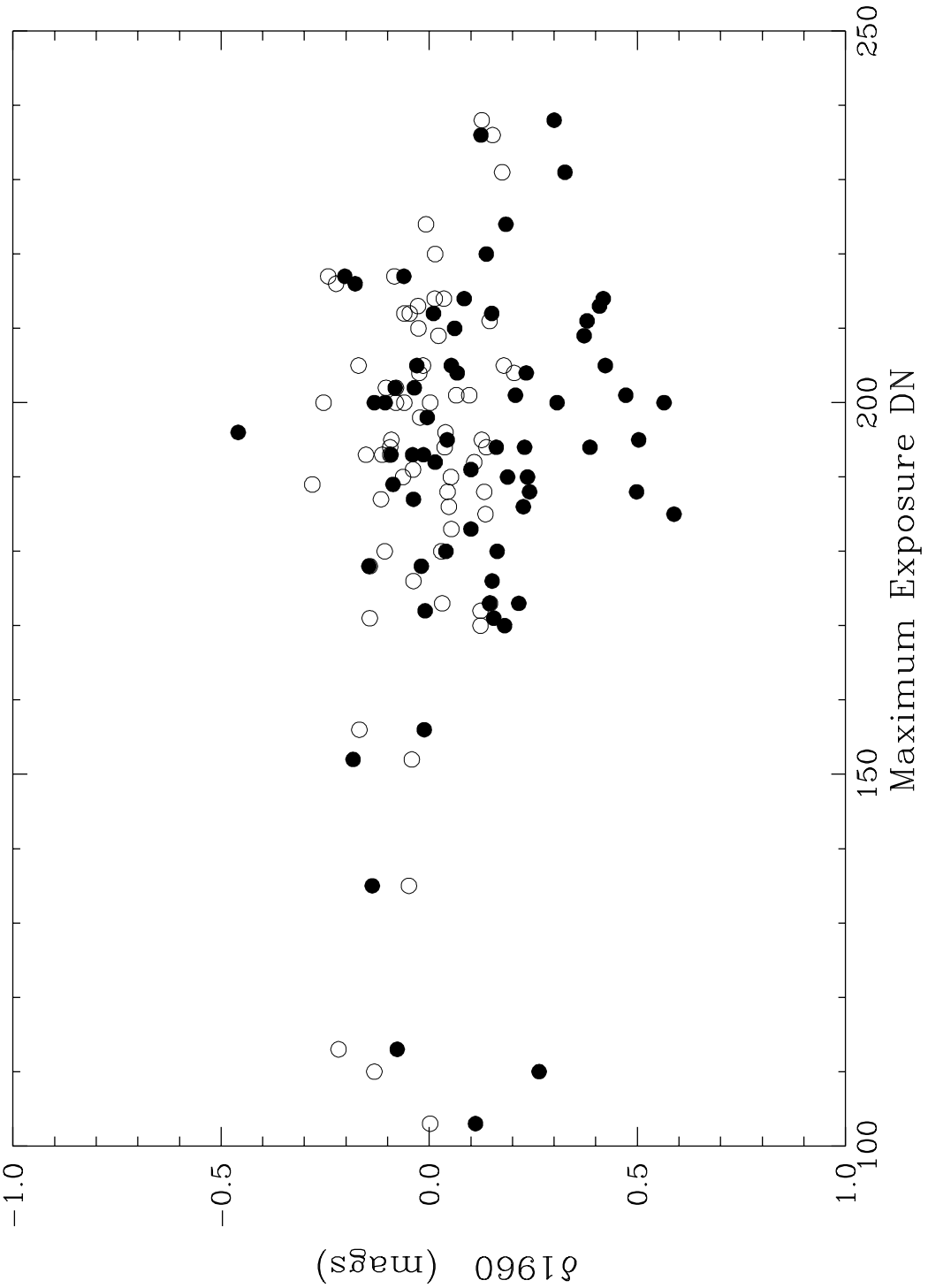

Figure 10d

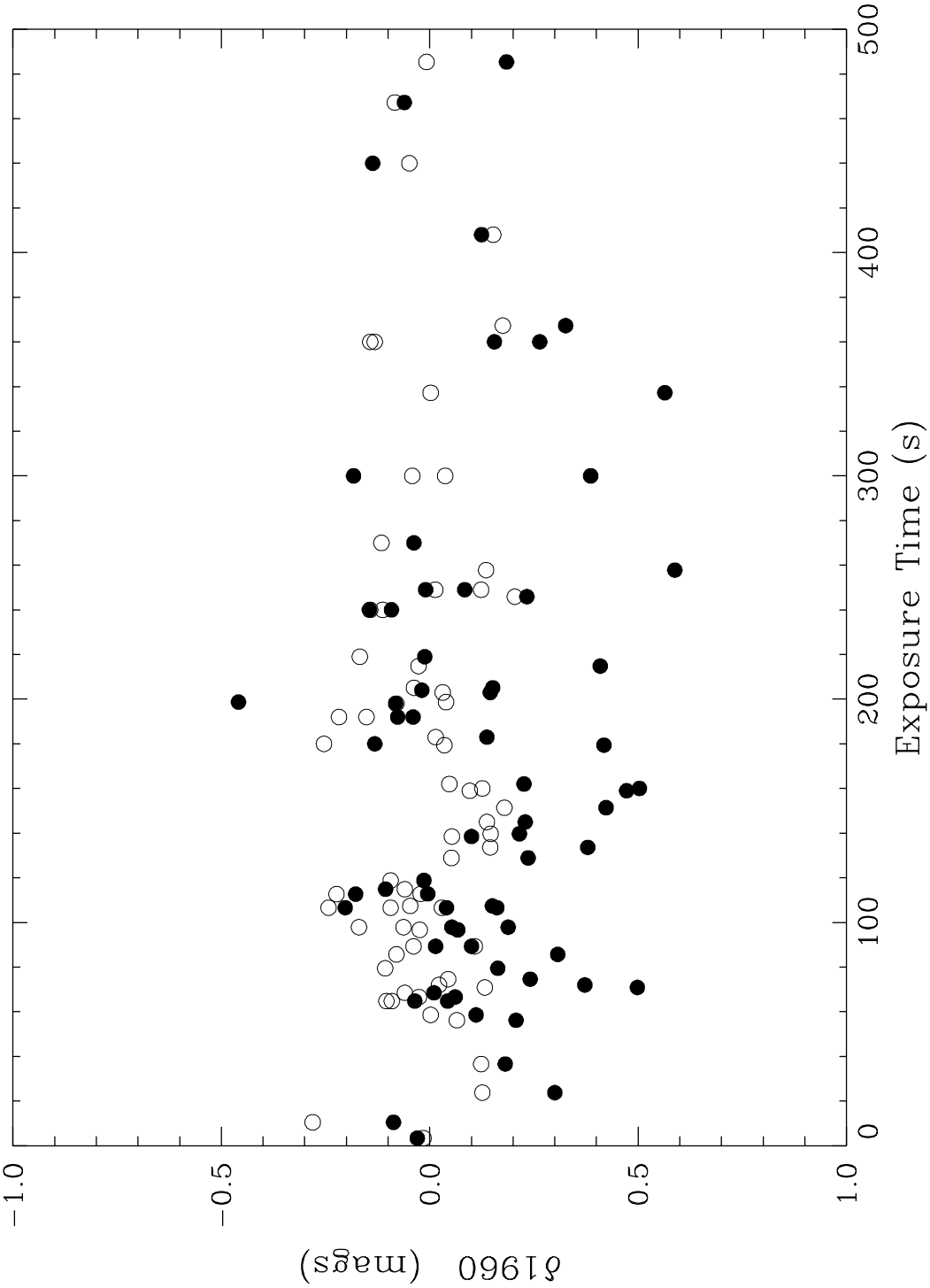

Figure 10e

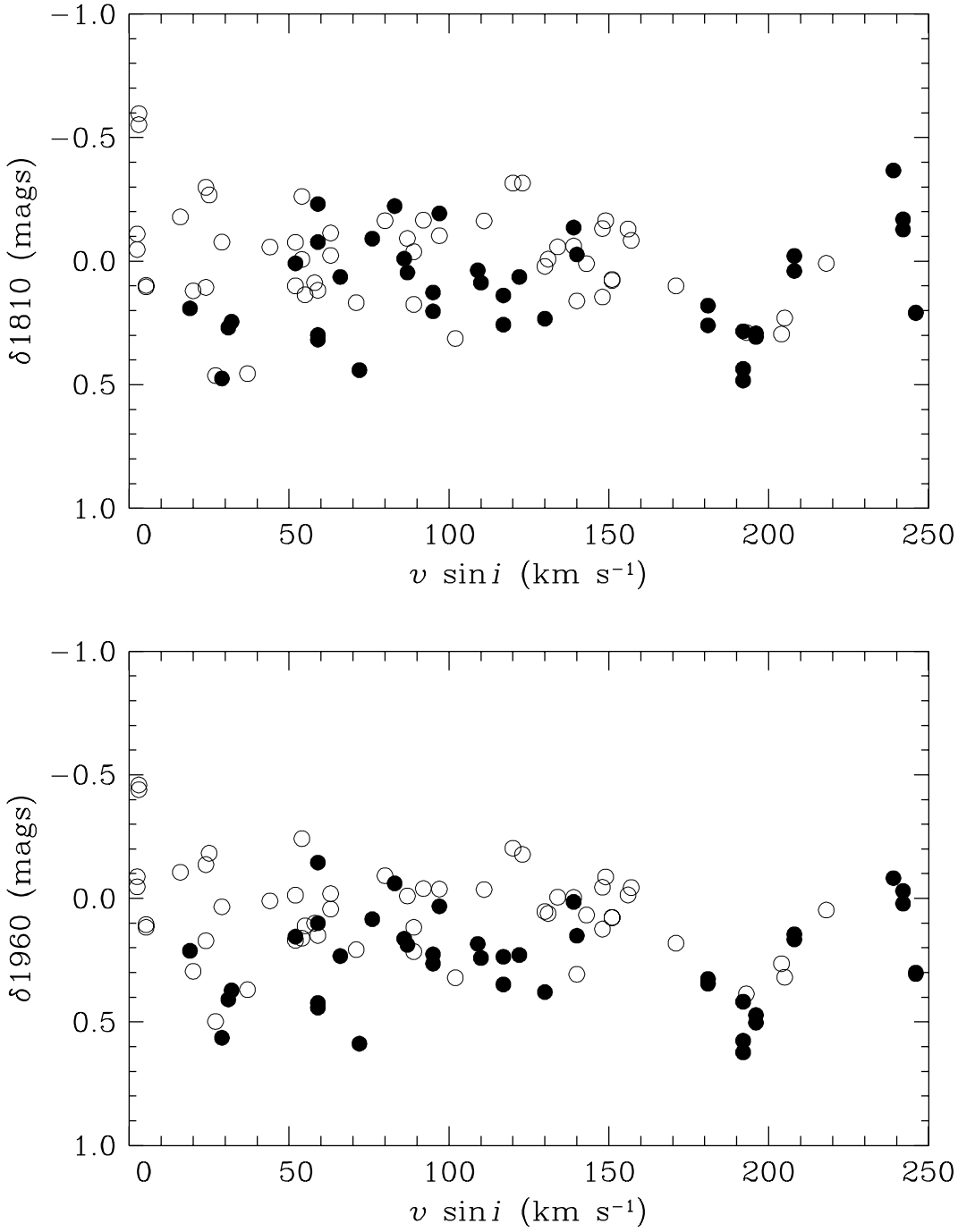

Figure 11

Fig. 11.— (a) The deviations in color at 1810Å versus the stellar rotation speed. *Filled circles*: stars inside the A–star gap. *Open circles*: stars outside the gap. (b) Same as (a) at a wavelength of 1960Å.

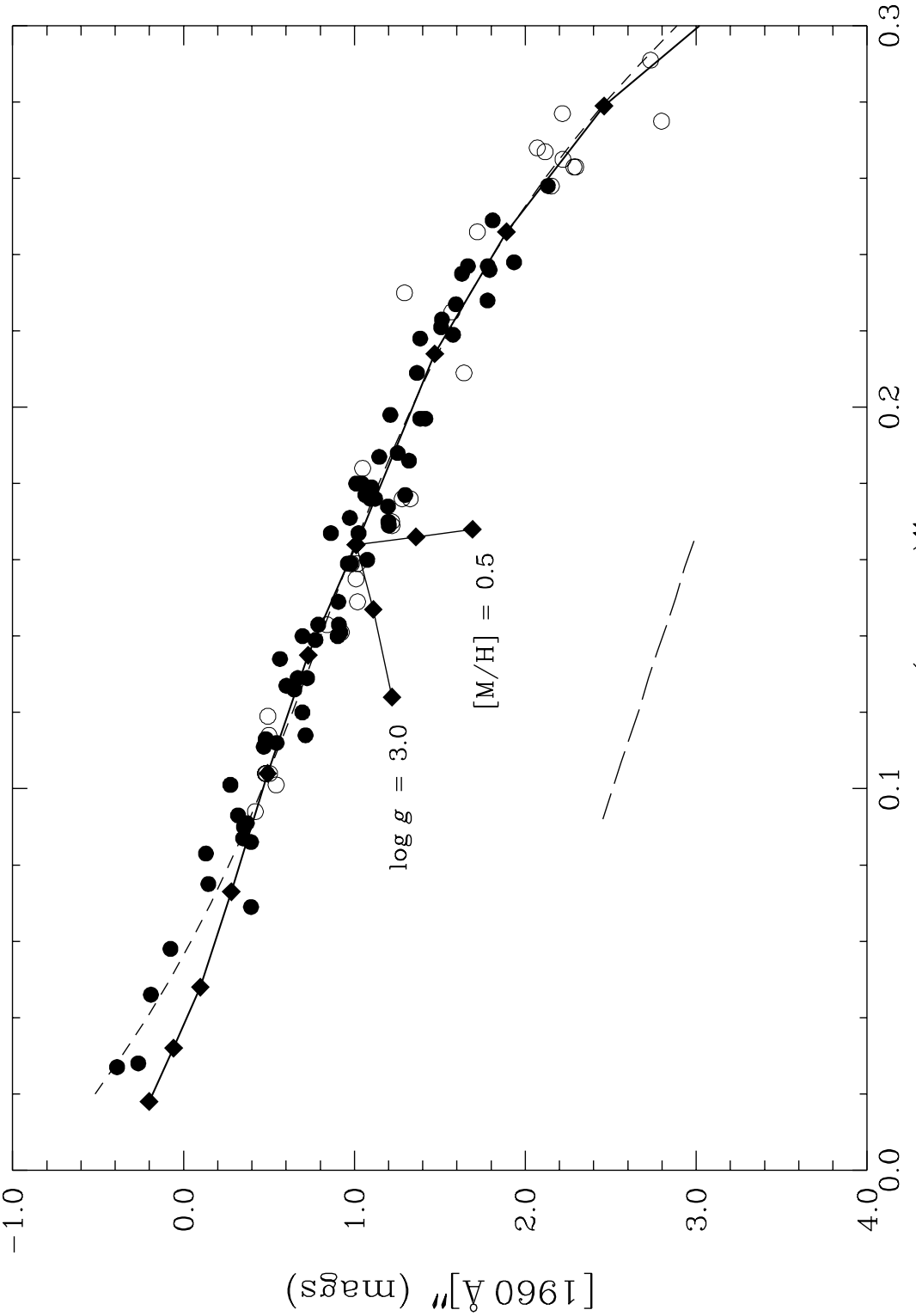

Figure 12

Fig. 12.— Two–color plot for luminosity– and metallicity–corrected colors. *Filled circles*: new spectra obtained here. *Open circles*: spectra taken from archives. *Filled diamonds*: ATLAS9 models. The long-dashed line is the interstellar reddening line. The short-dashed line is a cubic polynomial fit to the observations.

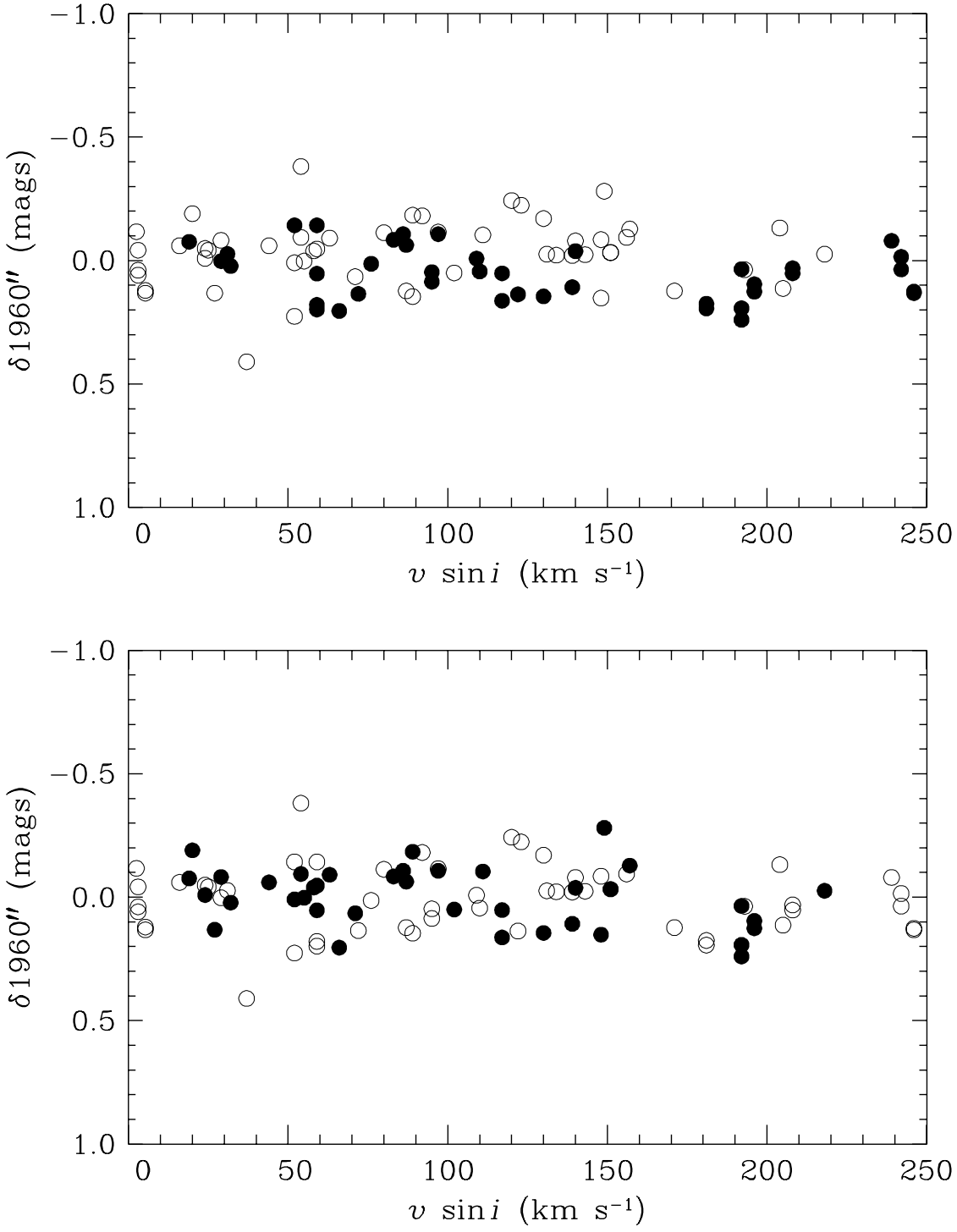

Figure 13

Fig. 13.— Deviations in adjusted 1960Å colors as a function of stellar rotation. (a) for stars inside the A–star gap (*filled circles*) and those outside the gap (*open circles*). (b) for double stars (*filled circles*) and single stars (*open circles*).

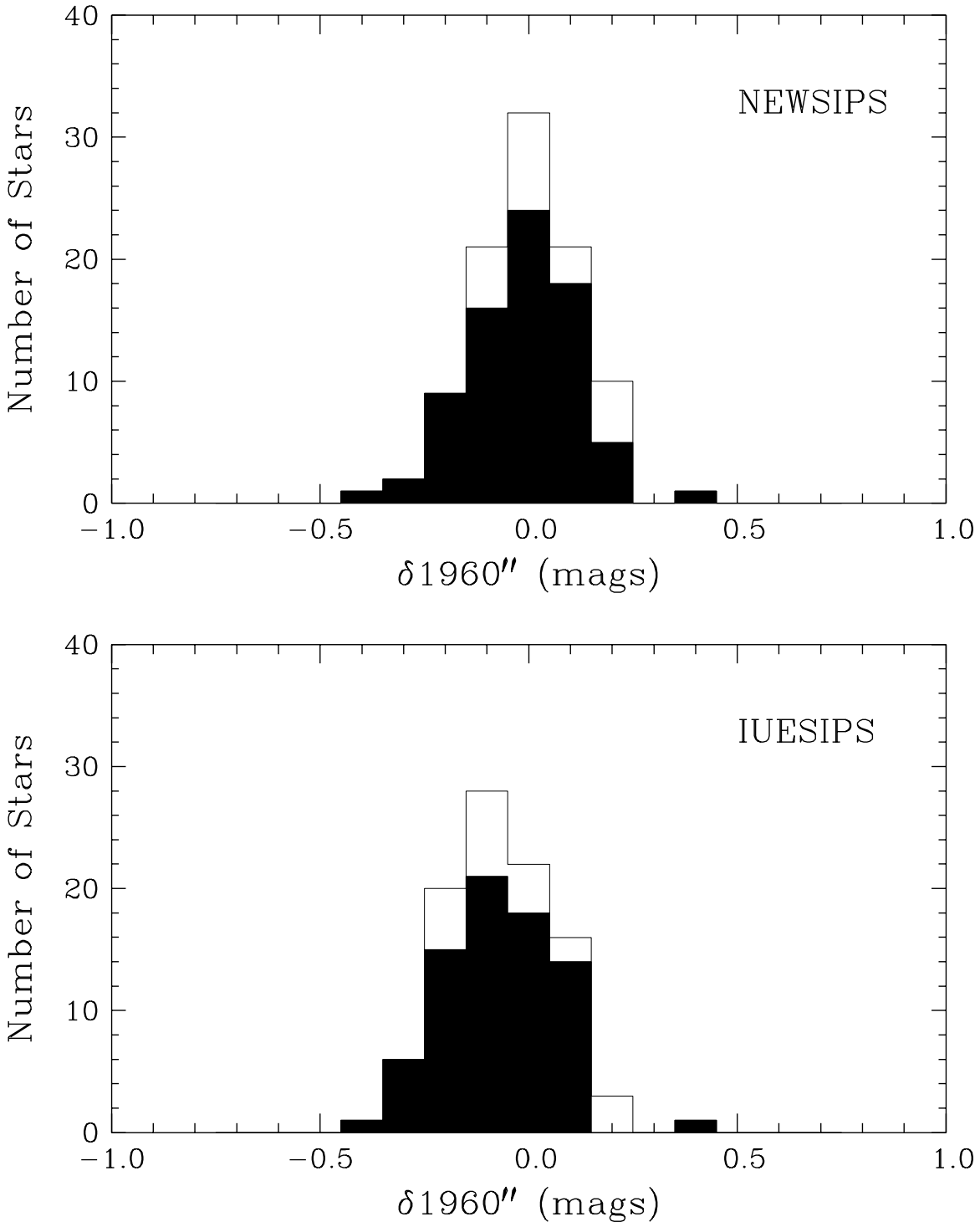

Figure 14

Fig. 14.— A stacked-bar histogram of the deviations in corrected 1960Å colors for non-variable stars (*filled area*) and for known δ Sct pulsators (*open area*). (a) For the NEWSIPS reductions. (b) For the IUESIPS reductions.

TABLE 1

Optical Photometry of Stars Observed by *IUE*

Star	HD	HR	V	$B-V$	β	$b-y$	c_1	m_1	δc_1	δm_1	$T_{\rm eff}$	Notes
23 And	905	41	5.72	0.31	2.717	0.222	0.613	0.156	0.032	0.021	7008	
θ Tuc	3112	139	6.13	0.23	2.817	0.147	0.984	0.187	0.170	0.004	7813	DS
π Cas	4058	184	4.94	0.18	2.857	0.085	0.901	0.228	0.017	−0.018	8173	SB2O
θ Cas	6961	343	4.33	0.17	2.845	0.087	0.997	0.213	0.137	−0.009	8076	SB
η Hor	16555	778	5.31	0.27	2.763	0.173	0.762	0.170	0.056	0.016	7342	
μ Cet	17094	813	4.26	0.31	2.749	0.189	0.762	0.187	0.084	−0.001	7236	SBO, VB
μ Hor	19319	934	5.11	0.34	2.701	0.223	0.635	0.152	0.102	0.015	6902	
HR 943	19545	943	6.19	0.16	2.869	0.094	0.899	0.196	−0.009	0.001	8284	
HR 1014	20888	1014	6.05	0.13	2.888	0.071	0.947	0.205	0.037	−0.009	8439	
χ^1 For	21423	1042	6.39	0.08	2.894	0.040	0.963	0.188	0.068	−0.008	9023	
κ Ret	22001	1083	4.72	0.40	2.671	0.260	0.507	0.152	0.065	0.013	6698	
HR 1104	22634	1104	6.75	0.17	2.867	0.092	0.991	0.192	0.087	0.003	8273	
δ Hor	26612	1302	4.93	0.33	2.713	0.212	0.773	0.169	0.204	0.010	6914	
51 Tau	27176	1331	5.65	0.28	2.767	0.175	0.787	0.185	0.073	0.006	7389	SBO
57 V483 Tau	27397	1351	5.59	0.28	2.766	0.172	0.771	0.193	0.059	−0.001	7385	DS, SB1?
δ^2 Tau	27819	1380	4.80	0.15	2.857	0.081	0.981	0.210	0.097	−0.007	8189	SB
υ Tau	28024	1392	4.28	0.26	2.753	0.165	0.947	0.175	0.261	0.012	7222	DS, SB1
71 V777 Tau	28052	1394	4.49	0.25	2.767	0.150	0.934	0.188	0.220	0.004	7348	DS, SBO
83 Tau	28556	1430	5.40	0.26	2.795	0.154	0.814	0.201	0.044	−0.004	7635	SB?
ρ Tau	28910	1444	4.65	0.25	2.797	0.144	0.823	0.205	0.049	−0.005	7642	DS, SB2O
α Cae	29875	1502	4.45	0.34	2.734	0.211	0.617	0.170	−0.022	0.009	7158	
β Pic	39060	2020	3.85	0.17	2.859	0.094	0.891	0.196	0.003	0.005	8200	
η Lep	40136	2085	3.71	0.33	2.720	0.221	0.622	0.157	0.032	0.012	7031	
μ Ori	40932	2124	4.12	0.16	2.854	0.093	0.981	0.200	0.103	0.000	8163	SB1O
α Pic	50241	2550	3.27	0.21	2.789	0.126	0.997	0.175	0.239	0.023	7526	
QW Pup	55892	2740	4.49	0.32	2.705	0.219	0.638	0.154	0.093	0.010	6892	
δ Gem	56986	2777	3.53	0.34	2.712	0.221	0.696	0.156	0.130	0.019	6932	SBO
ι UMa	76644	3569	3.14	0.19	2.843	0.104	0.856	0.216	0.000	−0.012	8063	SBO
18 DD UMa	79439	3662	4.83	0.19	2.833	0.113	0.892	0.196	0.052	0.006	7973	DS, SB
HR 3756	81919	3756	6.65	0.20	2.828	0.117	0.977	0.185	0.145	0.014	7923	VB
23 UMa	81937	3757	3.67	0.33	2.733	0.211	0.752	0.180	0.117	−0.004	7100	
HR 3761	82068	3761	6.05	0.15	2.851	0.076	0.975	0.194	0.103	0.010	8137	
υ UMa	84999	3888	3.80	0.29	2.736	0.196	0.830	0.162	0.184	0.017	7103	DS
21 LMi	87696	3974	4.48	0.18	2.836	0.111	0.870	0.196	0.026	0.007	8000	
HR 3991	88215	3991	5.31	0.36	2.702	0.235	0.557	0.160	0.021	0.012	6900	SB1O
LW Vel	88824	4017	5.28	0.25	2.778	0.155	0.855	0.184	0.119	0.011	7468	DS
HR 4086	90132	4086	5.33	0.25	2.781	0.147	0.838	0.185	0.096	0.011	7501	
30 LMi	90277	4090	4.74	0.25	2.779	0.151	0.956	0.195	0.218	−0.001	7451	
HR 4102	90589	4102	4.00	0.35	2.698	0.234	0.558	0.166	0.035	0.005	6863	SB
37 UMa	91480	4141	5.16	0.34	2.716	0.228	0.574	0.159	−0.004	0.016	7018	
49 UMa	95310	4288	5.08	0.24	2.793	0.145	1.007	0.194	0.241	0.000	7571	
ι Leo	99028	4399	3.94	0.41	2.686	0.267	0.606	0.172	0.123	−0.005	6731	SB1O
γ Crt	99211	4405	4.08	0.21	2.821	0.117	0.900	0.192	0.078	0.011	7862	
67 DP UMa	104513	4594	5.21	0.26	2.770	0.171	0.759	0.186	0.039	0.007	7424	DS
α Crv	105452	4623	4.02	0.32	2.705	0.216	0.586	0.157	0.041	0.016	6913	
78 UMa	113139	4931	4.93	0.36	2.708	0.244	0.578	0.168	0.024	0.002	6945	
80 UMa	116842	5062	4.01	0.16	2.847	0.097	0.928	0.192	0.064	0.010	8098	SB
22 Boo	126661	5405	5.39	0.23	2.817	0.121	0.976	0.236	0.162	−0.034	7813	

TABLE 1—*Continued*

Star	HD	HR	V	$B-V$	β	$b-y$	c_1	m_1	δc_1	δm_1	$T_{\rm eff}$	Notes
26 Boo	127739	5434	5.92	0.35	2.699	0.237	0.646	0.174	0.120	−0.002	6870	
σ Boo	128167	5447	4.46	0.36	2.681	0.253	0.488	0.132	0.020	0.038	6744	
ρ Oct	137333	5729	5.57	0.11	2.887	0.072	1.026	0.161	0.114	0.031	8439	
υ Ser	141187	5870	5.71	0.09	2.882	0.052	1.008	0.172	0.083	0.028	8397	
CL Dra	143466	5960	4.95	0.26	2.761	0.178	0.776	0.188	0.074	0.002	7339	DS, SB
ι^1 Nor	143474	5961	4.63	0.24	2.813	0.139	0.834	0.175	0.028	0.024	7796	VB
HR 6037	145689	6037	5.75	0.15	2.884	0.069	0.911	0.215	−0.009	−0.015	8409	
υ Oph	148367	6129	4.63	0.17	2.854	0.091	0.871	0.212	−0.007	−0.009	8158	SBO, VB
53 Her	152598	6279	5.32	0.29	2.708	0.208	0.630	0.164	0.080	0.018	7128	
69 Her	156729	6436	4.65	0.05	2.888	0.017	1.071	0.174	0.161	−0.001	9123	SB
44 Oph	157792	6486	4.17	0.28	2.794	0.168	0.787	0.207	0.019	−0.013	7632	
47 Oph	157950	6493	4.53	0.41	2.681	0.255	0.562	0.152	0.094	0.019	6707	SB2O
ν^1 Dra	159541	6554	4.88	0.26	2.777	0.173	0.768	0.183	0.034	0.010	7484	SB
ξ Ser	159876	6561	3.54	0.26	2.790	0.152	0.890	0.203	0.130	−0.007	7560	DS, SBO
HR 6618	161693	6618	5.75	0.01	2.877	0.016	1.150	0.148	0.226	0.019	9191	
HR 6749	165189	6749	4.95	0.22	2.825	0.129	0.827	0.194	−0.001	0.006	7906	SB
HR 7012	172555	7012	4.79	0.20	2.834	0.112	0.837	0.203	−0.004	0.004	8021	
ζ^1 Lyr	173648	7056	4.36	0.19	2.853	0.101	0.992	0.230	0.116	−0.026	8156	SB1O
θ Cyg	185395	7469	4.48	0.38	2.689	0.261	0.506	0.158	0.014	0.010	6809	
α Aql	187642	7557	0.77	0.22	2.828	0.137	0.880	0.178	0.048	0.018	7892	
η Ind	197157	7920	4.51	0.27	2.783	0.160	0.746	0.199	0.000	−0.002	7543	
ψ Cap	197692	7936	4.14	0.43	2.670	0.271	0.481	0.157	0.041	0.014	6643	
τ Cyg	202444	8130	3.72	0.39	2.685	0.256	0.607	0.165	0.127	0.005	6721	SB
α Cep	203280	8162	2.44	0.22	2.808	0.125	0.936	0.190	0.140	0.011	7721	
IK Peg	204188	8210	6.07	0.22	2.806	0.142	0.777	0.199	−0.015	0.002	7743	DS, SBO
74 Cyg	205835	8266	5.01	0.18	2.820	0.122	0.970	0.172	0.150	0.027	7844	
κ Peg	206901	8315	4.13	0.43	2.670	0.280	0.550	0.149	0.110	0.019	6609	SB1O
δ Ind	208450	8368	4.40	0.28	2.763	0.167	0.859	0.182	0.153	0.009	7331	VB
ϵ Cep	211336	8494	4.19	0.28	2.757	0.169	0.787	0.192	0.093	−0.003	7300	DS, SB
9 Lac	214454	8613	4.63	0.24	2.766	0.142	0.948	0.174	0.236	0.018	7337	SB
β Oct	214846	8630	4.15	0.20	2.819	0.110	0.908	0.198	0.090	0.005	7842	SB
7 And	219080	8830	4.52	0.29	2.742	0.181	0.723	0.172	0.059	0.012	7205	SB
τ Peg	220061	8880	4.60	0.17	2.808	0.104	1.013	0.166	0.217	0.036	7716	DS
λ Psc	222603	8984	4.50	0.20	2.822	0.103	0.892	0.204	0.069	0.001	7964	SB
82 HT Peg	223781	9039	5.30	0.18	2.835	0.099	0.967	0.181	0.124	0.022	7990	DS
HD 224638	224638	···	7.49	0.34	2.726	0.198	0.690	0.154	0.079	0.024	7030	GD

NOTE.—DS = δ Sct variable. GD = γ Dor variable. SB = spectroscopic binary. VB = visual binary